

# THE MOLECULAR GAS—STAR FORMATION CONNECTION IN AN OPTICALLY-SELECTED SAMPLE OF INTERACTING GALAXIES

HOWARD A. BUSHOUSE<sup>1</sup>, STEVEN D. LORD<sup>2</sup>, SUSAN A. LAMB<sup>3</sup>, MICHAEL W. WERNER<sup>4</sup>, AND  
 K. Y. LO<sup>5,6</sup>

03 Nov 1999 version, submitted to ApJ

## ABSTRACT

We have obtained <sup>12</sup>CO (1–0) emission-line observations for a sample of 37 interacting galaxy systems, chosen from a parent sample of optically-selected interacting galaxies. The sample observed here spans a large range of interaction strengths and current star formation rates. Using the standard Galactic CO-to-H<sub>2</sub> conversion factor we find that the interacting galaxies are, on average, marginally more rich in molecular gas than a comparison sample of isolated spiral galaxies, having mean  $M_{\text{H}_2}/L_B$  and  $M_{\text{H}_2}/M_{\text{HI}}$  ratios that are 20–40% higher than that of the isolated spirals. The interacting galaxies have a mean  $L_{\text{IR}}/M_{\text{H}_2}$  ratio that is a factor of  $\sim 1.3$  higher than the isolated spirals, indicating that the rate of high-mass star formation per unit molecular gas—the star formation efficiency—is also enhanced within the interacting galaxy sample. There is a strong correlation between relative H<sub>2</sub> content and star formation rates derived from both far-infrared and H $\alpha$  luminosities, indicating that the level of interaction-induced star formation activity is highly dependent upon the available gas supply. There are some individual galaxies with moderate amounts of molecular gas but little or no current star formation activity. Therefore molecular gas is a necessary, but not sufficient, condition for interaction-induced star formation activity. There is a strong correlation between interaction strength and both star formation rate and fractional H<sub>2</sub> content, with merging systems showing the highest star formation rates and fractional H<sub>2</sub> contents. There is also an increase in the molecular to atomic gas ratio with increasing interaction strength. If the increase in derived H<sub>2</sub> content is real, there must be a substantial conversion of H I to H<sub>2</sub> gas taking place in the strongest interactions. At least some portion of these trends, however, may arise due to an increase in cloud heating, brought about by the increased population of young, massive stars in galaxies with high current star formation rates. A reduction in the standard CO-to-H<sub>2</sub> conversion ratio by a factor of two could account for the systematic increase in derived H<sub>2</sub> content as a function of interaction strength. Such a change could not, however, account for the total range of H<sub>2</sub> contents within the entire samples of galaxies. Therefore the correlation between molecular gas content and star formation rate must be real.

*Subject headings:* galaxies: evolution — galaxies: interactions — galaxies: ISM — galaxies: starburst  
 — ISM: molecules — infrared: galaxies

## 1. INTRODUCTION

Studies of the global molecular gas content in interacting galaxy systems have shown that, on average, these galaxies appear to be rich in molecular gas and have star formation efficiencies—as measured by the formation rate of high-mass stars per unit molecular gas mass—that are much higher than those in isolated spiral galaxies (Sanders et al. 1986; Solomon & Sage 1988; Tinney et al. 1990; Sanders, Scoville, & Soifer 1991; Sofue et al. 1993; Young et al. 1996). Furthermore, both molecular gas content and star formation efficiency (SFE) appear to be correlated with interaction strength, with strongly interacting and merging systems having the highest molecular gas contents and SFE's.

Most of these studies have focused on samples of galaxies that were chosen for their high far-infrared fluxes, since

the observed correlation between infrared and CO flux (e.g. Young et al. 1984, 1986; Sanders & Mirabel 1985; Solomon & Sage 1988) ensures detectability in CO surveys. The presence of interacting and merging galaxies in these surveys is a bi-product of the fact that the relative fraction of interacting galaxies increases with far-IR luminosity (e.g. Soifer et al. 1984; Kleinmann & Keel 1987; Sanders et al. 1987, 1988a, 1988b).

In this study we investigate the molecular gas content of a sample of interacting systems that were selected according to their optical morphology. Therefore this study differs from previous investigations of CO emission in interacting galaxies, which have for the most part concentrated on infrared-luminous and merger type objects. The systems that have been studied are part of a larger sample that was selected on the basis of optical morphological

<sup>1</sup>Space Telescope Science Institute, 3700 San Martin Dr., Baltimore, MD 21218; bushouse@stsci.edu

<sup>2</sup>Infrared Processing and Analysis Center, California Institute of Technology, M.S. 100-22, Pasadena, CA 91125; lord@ipac.caltech.edu

<sup>3</sup>Department of Physics, University of Illinois, 1110 W. Green St., Urbana, IL 61801; slamb@astro.uiuc.edu

<sup>4</sup>Jet Propulsion Laboratory, California Institute of Technology, M.S. 264-767, 4800 Oak Grove Dr., Pasadena, CA 91109; mww@ipac.caltech.edu

<sup>5</sup>Department of Astronomy, University of Illinois, 1002 W. Green St., Urbana, IL 61801; kyl@astro.uiuc.edu

<sup>6</sup>Current address: Academia Sinica Institute of Astronomy and Astrophysics, P.O. Box 1-87, Nankang, Taipei, Taiwan 115, R.O.C.; kyl@asiaa.sinica.edu.tw

evidence for strong tidal interactions and has been well studied at optical, infrared, and radio wavelengths. The goal of this study is not only to measure the molecular gas content of interacting galaxies, but more importantly to examine the relationship between gas content and star formation characteristics, as well as interaction strength. Questions that this study will address include whether or not a rich molecular gas disk is a prerequisite for a starburst in interacting systems or if enhanced molecular gas production is occurring; whether optically “dormant” pair members have molecular material present; how the molecular gas content, far-IR luminosity and colors, and optical indicators of star formation are related in strongly interacting galaxies; and what the relationship is between molecular and atomic gas content. By addressing these questions, we hope to achieve a better idea of the circumstances under which starbursts occur in interactions and thus of the mechanisms which trigger the burst.

## 2. THE SAMPLES

The galaxies for this study have been selected from the large sample of interacting systems compiled by Bushouse (1986). Members of this sample were originally chosen on the basis of optical morphology only, preferentially selecting systems with features characteristic of strong interactions, such as tidal tails, loops, and bridges. Hence it is not intentionally biased towards infrared- or radio-bright systems, nor galaxies containing active galactic nuclei (AGN’s), although many systems in the parent sample do have these characteristics. Another advantage in choosing systems from this sample is that an extensive and well-studied database of optical spectra,  $H\alpha$  images, near- and far-IR photometry and imaging, and H I 21 cm data exists (Bushouse 1986, 1987; Bushouse, Lamb, & Werner 1988; Bushouse & Werner 1990; Bushouse, Telesco, & Werner 1998).

We have obtained  $^{12}\text{CO}$  (1–0) observations for 24 systems from the sample of Bushouse (1986). Some of the observed systems were selected because of their relatively high far-IR fluxes, which, because of the well-known correlation between far-IR and CO fluxes for galaxies, suggested that they would be easily detectable in the CO emission line. Other systems observed in this study were chosen in an attempt to fully sample the parameter space of known optical, infrared, and radio characteristics of the class of interacting galaxies. For example, while infrared-bright systems often have optical indicators of high current star formation rates (SFR’s), some systems were chosen because they have optical indications of low SFR’s, regardless of their infrared flux levels. Others were chosen because they have optical indicators of high current SFR’s, yet have low far-IR emission levels. Many systems were also chosen because of the relatively large angular separation of the two galaxies in the pair, allowing separate CO measurements for each of the galaxies and subsequent analysis of the properties of the individual galaxies.

We also searched the literature for CO observations of systems contained in the Bushouse (1986) parent sample. This search yielded a total of 19 observations of galaxies in 13 interacting systems. Most of these data are for

infrared-bright systems, as previous studies mainly used IR-selected samples. The combined sample of interacting systems analyzed in this study is not complete in either a flux-limited or volume-limited sense; rather, the galaxies were selected to span a wide range of parameter space, including far-IR flux level and optical indications of star formation properties.

Table 1 contains the list of interacting systems from the sample of Bushouse (1986) for which CO observations have been obtained. It also contains a comment on the nature of each system and the CO observations that have been obtained. There are a total of 19 paired systems, referred to as “complete pairs”, for which individual CO observations of the two galaxies in each pair are available. There are another 5 systems for which data for only one of the two galaxies (“1 of 2”) in the pair has been obtained. Finally, there are 13 systems that have a single CO observation that encompasses the entire pair. Nine of these are compact systems in which the pair of galaxies fits within a single CO aperture. The remaining four systems—NGC 1614, UGC 966, UGC 4509, and UGC 8387—are generally accepted to be systems that are in an advanced stage of merging, where the two original galaxies are in the process of coalescing into a single object. CO emission has been detected in 41 of the 56 observations.

We have also used a sample of isolated spiral galaxies from the Five College Radio Astronomy Observatory (FCRAO) Extragalactic CO Survey (Young et al. 1995) as a comparison sample in our study of the interacting systems. We selected 80 galaxies from this survey, ranging in morphological type from S0 to Sd, intentionally excluding irregulars and known interacting systems. The galaxies were chosen simply on the basis of available *IRAS* and CO observations.

## 3. OBSERVATIONS

The  $^{12}\text{CO}$  (1–0) observations were obtained in December 1988 using the 12 m NRAO telescope<sup>7</sup> (HPBW =  $55''$  at 115 GHz) on Kitt Peak. The telescope was equipped with dual polarization SIS receivers ( $T_{\text{ssb}} \sim 110$  K). Two 256 x 2 MHz channel filter banks, one for each polarization, provided a total velocity coverage of approximately  $1360 \text{ km s}^{-1}$  with a resolution of  $\sim 5.6 \text{ km s}^{-1}$  per channel. Telescope pointing was monitored by observations of planets and was estimated to be accurate to  $\pm 4''$  (rms). All of the observations were taken using the nutating sub-reflector, which gave very flat baselines. The spectra were calibrated using an ambient temperature chopper wheel and scaled by the telescope efficiency on a spatially extended source,  $\eta_{\text{fss}} = \eta_{\text{Moon}}$  to give line temperatures  $T_R^*$ . After co-adding both polarizations, the CO spectra were Gaussian smoothed to a resolution of  $15\text{--}20 \text{ km s}^{-1}$ , giving an average rms noise of 3–4 mK per channel.

The CO spectra were obtained with the spectrometer bandpass centered on the known H I or optical redshift. In cases of weak detections, the center of the spectrometer bandpass was shifted by a few hundred  $\text{km s}^{-1}$  while observing a given target, in order to confirm the reality of the detection. Observations were obtained for a single pointing at the optical coordinates of the galaxies. For systems

<sup>7</sup>The National Radio Astronomy Observatory is operated by Associated Universities, Inc., under contract with the National Science Foundation.

in which the two galaxies of the pair easily fit within the telescope half-power beam width ( $55''$ ), the telescope was pointed midway between the two galaxies. Most of the systems that were observed for this study are sufficiently distant that the total CO flux of the galaxies has been measured within a single telescope beam. We have not attempted to map any of the systems, nor apply any corrections to the observed fluxes for emission that might fall outside the beam area. Some of the data for interacting systems taken from the literature, however, are for more nearby systems with correspondingly larger angular sizes. The total line fluxes for many of these are the result of mapping observations.

The final co-added, baseline subtracted, smoothed spectrum for each detected source is shown in Fig. 1. The total CO intensity for each source was obtained by integrating the spectrum between velocity limits encompassing the observed line. Multiple independent flux measurements from the spectra show a  $1\sigma$  scatter of 3%. Independent observations of six galaxies within the interacting sample, also made with the NRAO 12m telescope (Zhu et al. 1999), yield a mean ratio in measured fluxes of 0.99, with a  $1\sigma$  scatter from object to object of 20%. We therefore estimate an uncertainty of 20% in the integrated CO flux for individual objects.

The integrated CO line fluxes for the interacting galaxies, converted from  $I_{\text{CO}}$  ( $\text{K km s}^{-1}$ ) to  $S_{\text{CO}}$  ( $\text{Jy km s}^{-1}$ ) using a gain factor of  $35 \text{ Jy K}^{-1}(T_R^*)$  for the NRAO 12 m telescope, are given in Table 1. Fluxes taken from the literature have been converted to the  $S_{\text{CO}}$  scale using the gain factor appropriate for the telescope that was used to obtain the data and are also shown in Table 1. The measured velocity centers and widths of the CO lines are also given.

A compilation of observed optical, *IRAS*, and H I data for the interacting systems included in this study is given in Table 2. *IRAS* fluxes have been measured using the Infrared Processing and Analysis Center’s one-dimensional coadding routine “SCANPI.” H I data are from a variety of sources, as noted in the table. Given the generally large beam sizes of the H I observations, most of these measurements are totals for each interacting system. H $\alpha$  fluxes are from our own spectral or narrow-band imaging observations (Bushouse 1987) or from the narrow-band imaging observations of Young et al. (1996). The H $\alpha$  imaging observations, which generally have a field of view of a few arc minutes, usually provide a global measurement for the galaxies in this sample, while the spectral observations used a  $22''$  diameter aperture and do not always sample an entire galaxy. Therefore the spectral data provide a lower limit on the total H $\alpha$  emission. All of the *IRAS* SCANPI measurements are global values for each system, therefore there is only one entry in Table 2 for each system. The H I and H $\alpha$  measurements that are totals for a pair are also listed with only one entry per system.

Table 3 presents derived parameters for the interacting galaxy sample. As with the observed data in Table 2, systems that have a global measurement for a given parameter are listed with a single entry. The far-IR luminosities,  $L_{\text{IR}}$ , were computed from the *IRAS* 60 and  $100 \mu\text{m}$  flux densities, using the procedure outlined in Appendix B of *Catalogued Galaxies and Quasars Observed in the IRAS Survey, Version 2* (Fullmer & Lons-

dale 1989). The far-IR luminosity, in solar units, is given by  $L_{\text{IR}} = 3.94 \times 10^5 D^2 [2.58 S_{60} + S_{100}]$ , where  $D$  is the distance in Mpc, and  $S_{60}$  and  $S_{100}$  are the *IRAS* flux densities listed in Table 2.

H $_2$  masses were derived from the CO (1–0) fluxes using a constant conversion factor of  $N(\text{H}_2)/I_{\text{CO}} = 2.8 \times 10^{20} \text{ H}_2 \text{ cm}^{-2} [\text{K}(T_R) \text{ km s}^{-1}]^{-1}$  (Bloemen et al. 1986). Kenney & Young (1989) show that this value of the conversion factor leads to H $_2$  masses in solar units given by  $M(\text{H}_2) = 1.1 \times 10^4 D^2 S_{\text{CO}}$ , where  $D$  is the distance in Mpc and  $S_{\text{CO}}$  is the CO flux in  $\text{Jy km s}^{-1}$ . We note that this conversion factor is derived from observations of Galactic molecular clouds and may not be universally applicable, especially in the case of strongly interacting galaxies where the state of the ISM could be substantially different than in the disk of a quiescent galaxy. For the sake of simplicity and consistency, the observational results and conclusions presented in §4 are based on the use of this constant conversion factor to derive H $_2$  gas masses from observed CO emission. At the very least, the derived values for H $_2$  gas mass can be thought of as a measure of the amount of warm (and therefore visible) CO gas in the galaxies. In §5 the possibility and ramifications of a variable conversion factor are discussed.

For the comparison sample of isolated galaxies, observed *IRAS* and H I data have been taken from the compilation of Young et al. (1989), CO fluxes from Young et al. (1995), and H $\alpha$  fluxes from Young et al. (1996). All derived properties for the isolated galaxies have been computed in the same fashion as for the interacting galaxies.

#### 4. RESULTS

In the following sections the molecular gas properties of the interacting systems are examined and compared to those of the sample of isolated spirals. First, the overall properties of the entire samples of interacting and isolated galaxies are compared, including an examination of the relationships between various global properties, such as luminosity, gas content, and star formation rates. The analysis is then continued by subdividing the interacting systems into smaller groups, based on star formation characteristics, pair separation, and interaction strength.

When analyzing properties of the interacting galaxies care is taken to utilize data for the individual galaxies within each system, when such are available. When comparing characteristics that are only available on a global basis with those for which individual measurements exist, the measurements for the individual galaxies within a system are combined to form a global value, so that the comparisons are consistent. For example, far-IR and H I measurements of the interacting systems typically include both galaxies in a pair, while CO and H $\alpha$  observations are available for many of the individual galaxies. Therefore when comparing far-IR and CO quantities, the CO measurements for the two galaxies in a pair are summed to compare with the global far-IR measurement.

For each relationship that is examined a least-squares linear fit to the data for only the isolated galaxies is computed, which then allows any unusual trends in the data for the interacting systems to be seen. All plots of these relationships show the computed fit to the isolated galaxy data, as well as the correlation coefficient of the fit.

#### 4.1. Properties of the Overall Samples

Mean and median properties of the entire isolated and interacting galaxy samples are listed in Table 4. Included in this table are dust temperatures derived by fitting *IRAS*  $S_{60}$  and  $S_{100}$  fluxes with a function of the form  $f_\nu \propto \nu^n B_\nu(T_d)$ , with  $n = 1.0$ , which is a common approximation for the broadband spectral energy distributions of galaxies. In order to properly take into account the non-detections in the samples, the mean and median statistics listed in Table 4 have been determined using the IRAF/STSDAS task “kmestimate,” which computes the Kaplan-Meier estimator of a randomly censored distribution (Kaplan & Meier 1958). Both mean and median values have been computed because they each have certain advantages. It is possible to estimate an uncertainty in the mean, but not the median. Knowing the uncertainties allows us to test the statistical significance of any differences between the samples. The median, on the other hand, is not as easily biased by a few extreme values, which are often present in the distributions analyzed here, and can therefore give a more appropriate representation of the overall sample.

##### 4.1.1. $H_2$ Content

The  $H_2$  content of the interacting galaxies, derived from the integrated CO emission, ranges from  $4 \times 10^8$  to  $5.6 \times 10^{10} M_\odot$ , with mean and median values of  $9.9 \pm 1.4 \times 10^9 M_\odot$  and  $6.4 \times 10^9 M_\odot$ , respectively<sup>8</sup>. There is complete overlap in the derived  $H_2$  gas mass values for the interacting and isolated galaxy samples, but the mean and median values for the interacting sample are factors of 2–3 times higher than those for the isolated galaxies (see Table 4). The larger values for the interacting sample, however, can in large part be attributed to observational factors. First, approximately 25% of the interacting galaxy CO observations are of compact or merging systems that include emission from more than one galaxy. Second, the interacting galaxy sample as a whole is biased towards more distant, and hence more luminous, galaxies; the blue luminosity,  $L_B$ , of the interacting sample is 1.5–2 times higher than that of the isolated galaxy sample. Fig. 2 shows that there is a strong correlation between  $L_B$  and  $M_{H_2}$ , therefore the overall increase in  $M_{H_2}$  for the interacting sample is not unexpected.

Furthermore, at the mean distance of the interacting galaxies, our CO detection limit corresponds to an  $H_2$  gas mass of  $\sim 2.5 \times 10^9 M_\odot$ , which is comparable to the median  $M_{H_2}$  of the isolated galaxy sample. Hence the distribution of  $M_{H_2}$  values for the interacting systems is biased upwards by our inability to detect low-mass systems. For example, excluding all Virgo cluster members from the sample of isolated galaxies—which eliminates most of the nearby systems in that sample—brings the ratios of mean and median  $M_{H_2}$  for the interacting and isolated galaxies down from 2–3 to  $\sim 1.5$ .

Normalizing the  $H_2$  content by  $L_B$  helps to remove the biases in the interacting galaxy sample introduced by sampling more than one galaxy at a time, as well as the overall increase in galaxy luminosity. The mean and median  $M_{H_2}/L_B$  ratios for the interacting systems are factors of  $1.8 \pm 0.3$  and 1.5 higher, respectively, than those of the

isolated galaxies. Much of this increase, however, can be attributed to our inability to detect interacting systems with small amounts of  $H_2$  at the greater distances of these systems. This is illustrated graphically in the histograms of  $M_{H_2}/L_B$  ratios for the two samples shown in Fig. 3. It can be seen from this figure that much of the increase in both mean and median  $M_{H_2}/L_B$  for the interacting systems is due to a lack of systems with low  $M_{H_2}/L_B$  values. Once again, excluding Virgo members from the isolated galaxy sample results in a drop in the mean and median ratios of  $M_{H_2}/L_B$  for the two samples to values of  $1.4 \pm 0.3$  and 1.0, respectively. The remaining increase in mean  $M_{H_2}/L_B$  mainly arises from a small number of interacting systems that have unusually high  $M_{H_2}/L_B$  ratios (see Fig. 3), several of which are the advanced merger systems that were identified in §2. Therefore there is only a marginal increase, on average, in fractional  $H_2$  content for the interacting systems, with a small number of systems showing a significant increase.

The correlation shown earlier between  $H_2$  content and  $L_B$  (see Fig. 2) indicates that, to first order, the amount of molecular gas is simply proportional to the overall size of a galaxy. Figure 4 shows that the total  $H_2$  and H I contents are similarly related. The correlation between  $H_2$  and H I, however, shows a larger scatter, especially for low-mass galaxies, where the molecular gas content can vary by almost two orders of magnitude for a given amount of atomic gas. The interacting and isolated galaxy samples have comparable mean  $H_2/H$  I ratios, while the median ratios indicate an increase of  $\sim 40\%$  in fractional  $H_2$  content for the interacting systems. Histograms of the  $M_{H_2}/M_{HI}$  ratios confirm that there is a similar distribution for the two samples (Fig. 5). The increase in median  $M_{H_2}/M_{HI}$  for the interacting galaxies again appears to be mainly due to a relative lack of systems with low values, rather than the presence of systems with higher than normal values. Note, however, that exclusion of the Virgo cluster members from the sample of isolated galaxies significantly reduces the mean  $M_{H_2}/M_{HI}$  ratio for that sample, due to the fact that the Virgo galaxies are systematically deficient in H I. Without the Virgo galaxies, the sample of isolated galaxies has a mean  $M_{H_2}/M_{HI}$  ratio that is a factor of  $1.2 \pm 0.3$  lower than that of the interacting galaxies.

##### 4.1.2. Star Formation Rate Versus $H_2$ Content

It is well established that the far-IR luminosity of a galaxy can be a good measure of its current SFR (see Kennicutt 1998 and references therein). Young, high-mass stars heat the interstellar dust within and around star forming regions and the warm dust then reradiates the stellar optical and UV light into the thermal infrared.  $H\alpha$  emission provides another measure of the current formation rate of high-mass stars (Kennicutt 1998). So in order to investigate the relationship between current star formation rate and molecular gas content in these galaxies, a comparison of their far-IR and  $H\alpha$  emission levels with derived  $H_2$  content has been performed.

As was found in previous CO surveys, there is a very good correlation between observed CO and far-IR fluxes and between derived  $H_2$  content and far-IR luminosity for both samples of galaxies (Fig. 6). The fact that the corre-

<sup>8</sup>All quoted errors are the  $1\sigma$  uncertainty in the mean.

lation exists for the observed fluxes as well as the derived luminosities and masses indicates that the  $L_{\text{IR}}$  versus  $M_{\text{H}_2}$  correlation is not simply a result of scaling the observed fluxes by the square of the distance to each system. It is also not simply due to far-IR emission and  $\text{H}_2$  content both increasing with galaxy size because Fig. 7 shows that there is still a strong correlation even after normalizing both  $L_{\text{IR}}$  and  $M_{\text{H}_2}$  by  $L_B$ . Many of the interacting systems—in particular all of the merging systems—lie above the mean relations defined by the isolated galaxies in Figs. 6 and 7. Indeed the overall  $L_{\text{IR}}/M_{\text{H}_2}$  and  $L_{\text{IR}}/L_B$  ratios for the interacting systems are factors of  $\sim 1.3$  and  $\sim 2.6$  higher, respectively, than that of the isolated galaxies. The  $L_{\text{IR}}/M_{\text{H}_2}$  and  $L_{\text{IR}}/L_B$  ratios also both tend to increase with increasing fractional  $\text{H}_2$  content.

The correlation between fractional far-IR luminosity and  $\text{H}_2$  content indicates that the current SFR in these galaxies is dependent upon the molecular gas supply. The fact that the interacting galaxies have a higher average  $L_{\text{IR}}/M_{\text{H}_2}$  ratio than the isolated galaxies further indicates that the amount of high-mass star formation activity per unit molecular gas (or star formation efficiency, as it is often called) is enhanced in these systems.

$\text{H}\alpha$  observations of the interacting systems have an advantage over the *IRAS* far-IR data in that  $\text{H}\alpha$  measurements are available for the individual galaxies within many of the pairs. Comparing the molecular gas and star formation rates of the individual galaxies is important because it has been shown that the two galaxies in an interacting pair can often have very different SFR's (e.g. Joseph et al. 1984; Bushouse 1987; Telesco, Wolstencroft, & Done 1988; Xu & Sulentic 1991). Figure 8 shows the relationships between observed  $\text{H}\alpha$  and CO fluxes, as well as derived  $\text{H}\alpha$  luminosities and  $\text{H}_2$  gas masses for the samples of interacting and isolated galaxies. In these figures the data for individual interacting galaxies have been plotted when available, however the data for compact and merging systems are still shown as global values. These figures indicate that there is a good correlation between total  $\text{H}\alpha$  luminosity and derived  $\text{H}_2$  content for these galaxies. A large part of this correlation, however, may be due to both  $\text{H}\alpha$  emission and  $\text{H}_2$  content scaling with galaxy size. Normalization by  $L_B$  should remove much of this bias. Figure 9 shows the relationship between  $L_{\text{H}\alpha}/L_B$  and  $M_{\text{H}_2}/L_B$  for the two samples. There is still a correlation, but a much weaker one (correlation coefficient  $r \sim 0.47$ ) than was seen when using  $L_{\text{IR}}$  as a measure of star formation.

The weaker correlation and increased scatter in the  $L_{\text{H}\alpha}/L_B$  versus  $M_{\text{H}_2}/L_B$  relation is likely due to variable amounts of internal extinction from galaxy to galaxy, which can have a dramatic effect on the  $\text{H}\alpha$  measurements. Many of the interacting galaxies in particular fall well below the mean relations between  $\text{H}\alpha$  and  $\text{H}_2$ , having low levels of  $\text{H}\alpha$  emission relative to their  $\text{H}_2$  content. A comparison of optical and near-infrared images of UGC 966 and UGC 12915, for example, shows that these galaxies suffer large amounts of extinction at optical wavelengths (Bushouse & Werner 1990). Others systems, such as UGC 4509, UGC 4881, and UGC 8528/8529, have unusually high  $L_{\text{IR}}/L_{\text{H}\alpha}$  ratios, which suggests that much of the star formation in these galaxies is occurring in embedded regions, so that any  $\text{H}\alpha$  emission associated with young stars is heavily extinguished. The relationship be-

tween  $L_{\text{IR}}/L_{\text{H}\alpha}$  and  $L_{\text{IR}}/L_B$  (Fig. 10) shows that most of these same galaxies scatter well above the mean relation, confirming that they have low levels of  $\text{H}\alpha$  emission relative to their far-IR luminosities. The high levels of far-IR emission from these galaxies indicates that they are experiencing significant star formation, but the  $\text{H}\alpha$  emission from the young stars is largely being obscured by dust.

#### 4.1.3. Star Formation Rate Versus $\text{H}_2$ Content for Individual Systems

An examination of the relationship between  $\text{H}_2$  content and star formation activity for the two galaxies within individual interacting pairs has also been performed. As mentioned above, the two galaxies within a given interacting pair often have very different levels of current star formation activity, and so an analysis of individual pairs will help to determine whether or not these disparities are associated with differences in molecular gas content. Far-IR and  $\text{H}\alpha$  emission measurements are again used as star formation indicators.

Unfortunately, few, if any, of the interacting pairs in this sample are resolved in the *IRAS* survey data, due to its low angular resolution. Thus the preceding comparisons of far-IR emission and molecular gas content were based on global values for each system. Bushouse, Telesco, & Werner (1998), however, have resolved the far-IR emission in six of the interacting pairs in the present sample using observations from the Kuiper Airborne Observatory. In addition, for some of the remaining widely-separated pairs, the *IRAS* Point Source Catalog (PSC) source location and error ellipse information can be used as an indication of the relative distribution of far-IR emission in the pairs. For example, in pairs where the PSC location and error ellipse are clearly associated with and confined to one of the galaxies, we assume that this galaxy is the dominant far-IR source. In others, where the *IRAS* PSC location is located between the optical locations of the galaxies, we assume that the far-IR emission is distributed more or less equally amongst the two galaxies.

There is a strong correlation between the relative levels of total far-IR and CO emission for the two galaxies in each of these six systems observed by Bushouse, Telesco, & Werner (1998). Four systems—UGC 5617/5620, UGC 7776/7777, UGC 8335, and UGC 11175—have one galaxy that is the dominant far-IR source, and in all cases this galaxy is also the dominant source of CO emission. In the other two systems—NGC 4038/4039 and UGC 8641/8645—both far-IR and CO emission are distributed approximately equally between the two galaxies in the pair. An analysis of the *IRAS* PSC positions for the remaining pairs in the samples shows that there are nine systems where the PSC position is clearly associated with or dominated by one of the two galaxies in the pair: Arp 248, Arp 256, UGC 480, UGC 6224, UGC 8528/8529, UGC 10923, UGC 11673, UGC 12699/12700, and UGC 12914/12915. In all of these pairs, the dominant far-IR galaxy is also the dominant or only source of CO emission. There are four pairs in which the far-IR emission is not clearly dominated by either of the two galaxies: UGC 813/816, UGC 6471/6472, UGC 7938/7939, and UGC 11284. In two of these pairs—UGC 7938/7939 and UGC 11284—the observed CO emission is also distributed nearly equally between the two

galaxies. In the UGC 813/816 and UGC 6471/6472 pairs, however, one of the two galaxies is the dominant source of CO emission by factors of 1.7 and 2.1, respectively.

H $\alpha$  measurements are available for the individual galaxies within a total of 15 of the interacting pairs. For all pairs in which one galaxy has a much higher current SFR—as indicated by total H $\alpha$  emission—than its companion (e.g. Arp 248, UGC 480, UGC 5617/5620, UGC 8335, UGC 10923, UGC 11175, and UGC 12699/12700) the active galaxy has moderate to large amounts of molecular gas, while its inactive companion has much lower or undetectable levels of H $_2$ . For pairs in which the two galaxies have similar SFR's (e.g. UGC 813/816, UGC 7776/7777, UGC 7938/7939, UGC 8641/8645, UGC 11284, and UGC 12914/12915), the two galaxies also have comparable levels of H $_2$  content.

At first glance these data would seem to indicate a strong correlation between molecular gas content and current star formation rates. However, a large part of this correlation appears to be due to a simple scaling of both parameters with overall galaxy size. In nearly every one of the interacting pairs mentioned above as having one galaxy as the dominant H $\alpha$ , far-IR, and CO source, this galaxy also has a much larger optical blue luminosity than its companion. In many cases the ratio of  $L_B$  values is comparable to the ratio of  $M_{H_2}$  values for the two galaxies. In the UGC 480, UGC 5617/5620, UGC 10923, UGC 11175, and UGC 12699/12700 pairs, for example, in which the  $L_B$  ratio of the two galaxies is a factor of 3 or greater, it is always the more luminous galaxy that is the dominant H $\alpha$ , far-IR, and CO emission source. On the other hand, there are also pairs such as UGC 7776/7777 and UGC 8335, in which the two galaxies have comparable optical luminosities and apparently similar morphological types, yet one galaxy in the pair is clearly dominant in H $\alpha$ , far-IR, and CO emission.

Therefore normalization by galaxy size is once again necessary in order to reveal any real trends between molecular gas content and star formation activity. Using  $L_B$  again as a normalization parameter, Figure 11 shows the  $L_{H\alpha}/L_B$  ratios as a function of  $M_{H_2}/L_B$  ratio for the 15 interacting pairs that have individual H $\alpha$  and CO measurements. Seven of the pairs included in this figure have one galaxy with detectable CO emission and the other without: Arp 248, UGC 480, UGC 5617/5620, UGC 8335, UGC 8528/8529, UGC 10923, and UGC 12699/12700. In each of these pairs the galaxy with detectable CO emission also has a (often substantially) larger  $L_{H\alpha}/L_B$  value. Of the remaining eight pairs that have detectable CO emission in both galaxies, only two—Arp 256 and UGC 7776/7777—show a strong correlation between fractional H $_2$  content and star formation, where the pair member with the higher  $M_{H_2}/L_B$  value also has a higher  $L_{H\alpha}/L_B$  value. In another three systems—UGC 813/816, UGC 7938/7939, and UGC 11284—the two galaxies have comparable amounts of star formation activity and molecular gas. The final three systems—UGC 8641/8645, UGC 11175, and UGC 12914/12915—do not show a strong correlation between SFR and H $_2$  content. Thus a large fraction of the available sample shows a clear dependence between current levels of star formation and molecular gas content, while there are a few systems that do not.

#### 4.2. Subsamples Based on Star Formation Activity

The sample of interacting galaxies consists of objects that span a large range of star formation activity, as indicated by both their optical and infrared properties. In this section the mean properties of three subsamples of the interacting galaxies are examined, where the subsamples are based on star formation properties. The subsamples are composed of galaxies with similar optical or infrared properties, and hence an analysis of their mean properties will help to reduce the inherent system-to-system scatter that has been seen in the preceding analyses.

The three subsamples are taken from a study of the far-IR properties of the parent sample of interacting galaxies by Bushouse, Lamb, & Werner (1988) and are listed in Table 5. The first group, labeled “High SFR-High IR”, are systems that have optical indications of high current SFR's (e.g. H II region like spectra and high H $\alpha$  emission) and high levels of far-IR emission. This group contains all of the merging systems in the interacting sample from this study, as well as other very strongly interacting systems. Systems in the “High SFR-Low IR” group, on the other hand, have optical indications of high SFR's, but little or no far-IR emission detected by *IRAS*. The “Low SFR” group consists of systems that have optical spectra with weak or undetectable emissions lines and a stellar continuum dominated by older G–M type stars. Because the *IRAS* data for the interacting systems do not resolve the individual galaxies within the pairs, care has been taken to select systems for these subsamples which contain galaxies with similar optical properties. The mean properties of the subsamples are listed in Table 6.

##### 4.2.1. High SFR, High IR Emission Galaxies

The galaxies in the High SFR-High IR group have all of the far-IR and molecular gas properties typically seen in IR-selected samples of galaxies. They have very high  $L_{IR}/L_B$  and  $L_{IR}/M_{H_2}$  ratios, which are signs of high SFR's and SFE's. They also appear to be very rich in molecular gas, as evidenced by the factor of four increase in the mean  $M_{H_2}/L_B$  ratio as compared to the isolated spirals. The ratio of molecular to atomic gas is also enhanced by a factor of  $\sim 3$  in these systems. The high H $_2$ /H I ratios are not due to lower levels of H I content, as the mean  $M_{HI}$  and  $M_{HI}/L_B$  are also both systematically higher for these systems than for the isolated galaxies.

##### 4.2.2. High SFR, Low IR Emission Galaxies

The High SFR-Low IR group galaxies, on the other hand, have very low levels of far-IR emission and appear to be nearly devoid of molecular gas. In fact none of these systems was detected in our CO observations. In this respect they conform well to the far-IR versus CO emission correlation. The mean global H $\alpha$  luminosity—and hence the current population of young, high-mass stars—in these systems is comparable to that of the isolated galaxy sample. The mean  $L_{H\alpha}/L_B$  ratio, however, is equal to that of the High SFR-High IR group of interacting galaxies and more than twice that of the isolated galaxies, which indicates that a much larger fraction of the total stellar populations of these galaxies is in young, high-mass stars. This is confirmed by the very large H $\alpha$  emission-line equivalent widths seen in the optical spectra of these galaxies

(Bushouse, Lamb, & Werner 1988). Yet they appear to have very little, if any, molecular gas to support this star formation activity. Thus the high-mass SFE, as measured by the  $L_{\text{H}\alpha}/M_{\text{H}_2}$  ratio, is the highest of any of the groups.

The High SFR-Low IR systems also have low blue luminosities and therefore may be intrinsically small or low-mass galaxies. However, they do contain reasonably large amounts of atomic hydrogen, resulting in a larger than normal mean  $\text{H I}/L_B$  ratio. The low blue luminosities of these galaxies suggests that they may be low metallicity systems, since metallicity appears to be correlated with galaxian mass (e.g. Pagel & Edmunds 1981; Garnett & Shields 1987; Vila-Costas & Edmunds 1992). Emission line ratios in the optical spectra of these galaxies support this conclusion. The mean O/H ratio derived from emission line measurements is a factor of 3.5 smaller than that of the High SFR-High IR systems. This is consistent with the lack of both far-IR emission and molecular gas. Lower metallicity is expected to be accompanied by a smaller dust abundance, which is necessary to reradiate the UV-optical light of high-mass stars into the far-IR. Since  $\text{H}_2$  is formed in a grain surface reaction, the lack of dust will also lower the  $\text{H}_2$  formation rate.

Alternatively, recent theoretical and observational evidence suggests that the  $\text{CO}/\text{H}_2$  ratio may be much lower than normal in low metallicity galaxies (e.g. Arnault et al. 1988; Maloney & Black 1988; Madden et al. 1997; Smith & Madden 1997). Low abundances of C and O and a low dust column density may result in deeper penetration of UV photons from high-mass stars, decreasing the size of the CO-emitting region within a molecular cloud, while  $\text{H}_2$  remains relatively self-shielded. This can result in large volumes of molecular clouds which are not sampled by CO observations, giving rise to an abnormally high CO-to- $\text{H}_2$  conversion factor. If this is the case, then the derived  $\text{H}_2$  contents for the High SFR-Low IR group of galaxies will be severely underestimated.

#### 4.2.3. Low SFR Galaxies

The Low SFR subsample is comprised of galaxies with optical luminosities and  $\text{H I}$  gas masses comparable to, or greater than, most of those in the whole isolated and interacting samples. The current SFR's in these systems, however, are very low, as can be seen from their low mean  $\text{H}\alpha$  luminosities and  $L_{\text{H}\alpha}/L_B$  ratios. In fact the mean  $L_{\text{H}\alpha}/L_B$  ratio is a factor of ten lower than that of the isolated spirals. Of the seven objects that have been observed in this subsample, CO emission has been detected from only two galaxies (UGC 480 West and UGC 11673 South). Therefore it appears that one of the main reasons for the lack of current star formation activity in these galaxies is a corresponding lack of molecular gas. Notice however, that the two galaxies that were detected in CO, have considerable amounts of molecular gas—more than many of the very active systems in the High SFR-High IR subsample. Thus not all inactive systems can be explained by a simple lack of molecular gas, but instead suggests that other specifics of the interaction events in which they are involved have failed to provide the necessary inducement for star formation activity.

#### 4.3. Subsamples Based on Interaction Strength

Previous studies of the molecular gas properties of small samples of interacting galaxies have indicated some correlations between interaction strength and both  $\text{H}_2$  content and  $L_{\text{IR}}/M_{\text{H}_2}$  ratios, where interaction strength was based on the proximity of companions and the degree of morphological disturbance. For example, Solomon & Sage (1988) found that weakly interacting galaxies have average  $L_{\text{IR}}/M_{\text{H}_2}$  and  $M_{\text{H}_2}/L_B$  ratios that are not substantially different than isolated galaxies, but strongly interacting and merging systems have significantly higher values of both quantities. Young et al. (1996) also found that the high-mass SFE, as measured by  $L_{\text{H}\alpha}/M_{\text{H}_2}$  ratios, is enhanced by a significant amount in strongly interacting—and in particular merging—systems, while weakly interacting pairs show no such increase. These studies, however, were based upon either IR-selected samples of galaxies, and thus may be biased towards galaxies with high molecular gas content, or sampled a relatively small range of interaction types and small numbers of systems.

We have performed a similar analysis using two different approaches. First, the projected separation of the galaxies in each interacting system has been used as a rough estimate of the strength or severity of the collisions. Figure 12 shows the relationship between pair separation and several derived quantities for the interacting systems. The  $S_{60}/S_{100}$  and  $L_{\text{IR}}/L_B$  ratios can both be used as indicators of current SFR's due to the increase in dust temperature from heating by massive stars, as well as a corresponding overall increase in far-IR dust emission. The relations shown in Figure 12 indicate that there is very little correlation between SFR and pair separation. There is only a modest increase in the average values of the  $S_{60}/S_{100}$  and  $L_{\text{IR}}/L_B$  ratios as separation decreases. The only connection that can be seen is the fact that no systems with large separations have higher than normal SFR's. Therefore small separations are a necessary but not sufficient condition for significant interaction-induced star formation activity.

Figure 12 shows the same behavior for the  $L_{\text{IR}}/M_{\text{H}_2}$  and  $M_{\text{H}_2}/L_B$  ratios as a function of pair separation. There is only a modest increase in the average values as pair separation decreases and no systems with large separations have elevated values. The absence of any obvious correlation between pair separation and these measures of star formation and molecular gas content indicates that either there is no correlation between interaction strength and induced star formation activity or that projected pair separation, by itself, is a poor indicator of interaction strength. The next approach will show that there is in fact a correlation between interaction strength and star formation activity and therefore we conclude that projected pair separation is simply a poor measure of interaction strength. This is not surprising since the observed pair separation always provides only a lower limit on the true separation due to projection effects. Furthermore, we may be seeing some strongly interacting systems at a late evolutionary stage when the two galaxies have already passed the point of closest approach.

The second approach that has been used is to classify the strength of the interactions based upon the morphological appearance of each system. The systems have been classified into five groups, using the following criteria.

- Class 1: Galaxies with nearby companions, but showing no obvious morphological disturbance.
- Class 2: Galaxies with nearby companions and modest morphological disturbances, but no tidal tails or bridges.
- Class 3: Galaxies with nearby companions and severe morphological disturbances, including tidal tails, bridges, loops, and streamers.
- Class 4: Galaxies in apparent contact with their companions and with severe morphological disturbances. Included in this category are a few systems which are not in physical contact at this time, but obviously suffered a head-on or nearly head-on collision in the recent past. For example, the UGC 12699/12700 pair exhibits a ring feature which must have been produced by a head-on collision, and is included in this category.
- Class 5: Merging systems, with a single amorphous body, possibly double nuclei, and a pair of remnant tidal tails. The four systems identified as mergers throughout the preceding analysis make up this category.

Table 7 lists the interacting systems that have been assigned to each class. Table 8 lists the mean properties of the classes, which are also displayed graphically in Figure 13. Several trends are evident. First, the far-IR luminosity,  $L_{\text{IR}}/L_B$  ratio, and dust temperature (as indicated by the  $S_{60}/S_{100}$  flux ratio) all increase systematically with interaction strength. The  $L_{\text{H}\alpha}/L_B$  ratio shows a similar trend, but drops back down somewhat in class 5 systems. This is almost certainly due to extremely large extinction effects on the observed H $\alpha$  emission in the very dusty class 5 merging systems. All of these trends are a clear indication of increased mean SFR's in the more strongly interacting systems. Second, there is a steady increase in the  $L_{\text{IR}}/M_{\text{H}_2}$  and  $L_{\text{H}\alpha}/M_{\text{H}_2}$  ratios (except again for the  $L_{\text{H}\alpha}/M_{\text{H}_2}$  ratio in class 5 systems), which indicates that the high-mass SFE also increases with interaction strength. Finally, there is an obvious correlation between interaction class and both  $M_{\text{H}_2}/L_B$  and  $M_{\text{H}_2}/M_{\text{HI}}$  ratios, indicating that the more strongly interacting systems have systematically larger amounts of molecular gas per unit optical luminosity and per unit atomic gas mass. Some of the apparent increase in  $M_{\text{H}_2}/M_{\text{HI}}$  for the class 5 systems could be due to underestimates of their H I emission fluxes. All of these systems show an absorption component in their H I spectra, due to the presence of strong nuclear radio sources (Bushouse 1987; Mirabel & Sanders 1989).

Notice that the largest changes in these properties often occur in the transitions from class 2 to 3 and again from class 4 to 5. The jump from class 2 to 3 indicates that a moderately strong interaction is necessary to have any significant effect on the galaxies, and the transition from class 4 to 5 indicates that mergers have the largest effect. The more subtle changes from class 3 to 4 may be partially due to the highly subjective nature of classifying the systems, which results in some mixing between the classes.

It is also interesting to note that all of the interacting systems identified in the previous section as having high

SFR's—both those with and without correspondingly high levels of far-IR emission—are members of class 3 or higher systems, with many being in classes 4 and 5. The systems identified as having low current SFR's, however, are all in the interaction strength class 2 category. This adds further support to our conclusion that, in addition to having a sufficient supply of molecular gas, it is necessary to have a moderately strong interaction in order to stimulate high levels of star formation activity.

## 5. DISCUSSION

Using the standard Galactic CO-to-H<sub>2</sub> conversion factor to estimate H<sub>2</sub> content we have found that there is a good correlation between fractional H<sub>2</sub> content and current star formation rates for the overall samples of isolated and interacting galaxies. Furthermore, galaxies with high current SFR's almost always have moderate to large amounts of H<sub>2</sub> gas to support that activity; the only exceptions being the low-metallicity galaxies with high SFR's but low far-infrared and CO emission levels. The fractional content of molecular gas for the entire sample of interacting galaxies, as measured by both their  $M_{\text{H}_2}/L_B$  and  $M_{\text{H}_2}/M_{\text{HI}}$  ratios, is also somewhat higher than that for the isolated galaxies, at a level of  $\sim 20\text{--}40\%$ . The fractional H<sub>2</sub> content of the interacting systems shows a steady increase, on average, with increasing interaction strength, with the most strongly interacting and merging systems having the largest increase relative to isolated galaxies.

Previous studies have also examined the relationship between molecular gas content and interaction strength or stage, which have yielded mixed results. Young & Knezek (1989) found enhanced molecular to atomic gas ratios in close pairs and mergers when compared to isolated spirals. In a study of infrared-luminous galaxies—most of which were in interacting pairs—Mirabel & Sanders (1989) also found that the H<sub>2</sub>/H I ratio increases with interaction strength and is highest in merging systems. On the other hand, more recent studies of infrared-luminous merging systems have found that the CO luminosity (and hence derived H<sub>2</sub> content) is either not correlated with interaction stage (Solomon et al. 1997) or actually decreases with decreasing pair separation (Gao 1996; Gao & Solomon 1999). Furthermore, in a study of the molecular gas properties of another optically-selected sample of interacting galaxies Horellou, Booth, & Karlsson (1999) find no correlation between molecular gas fraction and degree of morphological disturbance.

If there is an increase in H<sub>2</sub> content in the more strongly interacting systems, this would imply that H<sub>2</sub> is somehow being created by the interaction event, and that the process by which this occurs acts more strongly in the more strongly interacting and late-stage systems. Many models of interacting and merging systems have shown that a combination of gravitational torques and dissipative collisions will remove enough angular momentum from disk gas to produce radial inflows into the central regions of galaxies (e.g. Noguchi 1988, 1991; Olson & Kwan 1990; Mihos, Richstone, & Bothun 1992; Barnes & Hernquist 1992, 1996; Lamb, Gerber, & Balsara 1994; Gerber, Lamb, & Balsara 1996; Mihos & Hernquist 1996). The increase in density of this centrally concentrated gas, as well as the lower velocity dispersion that may result from settling into

the deeper potential well of the nucleus, may then give rise to enhanced H I-to-H<sub>2</sub> conversion processes (Young & Knezek 1989; Mirabel & Sanders 1989). Some of the models also indicate that the largest gas inflows will occur near the final stages of merging systems, consistent with our finding the highest H<sub>2</sub> contents in merging systems. The fact that interferometric observations of CO emission have revealed that the molecular gas in interacting galaxies is preferentially concentrated towards their nuclei, and that it becomes increasingly concentrated as a function of interaction strength (e.g. Sanders et al. 1988a; Sargent & Scoville 1991; Scoville et al. 1991; Lo, Gao, & Gruendl 1997; Gao & Solomon 1999) also tends to support this scenario.

There is, however, no direct evidence yet for this suggested increase in the H I-to-H<sub>2</sub> conversion process. Furthermore, some models have shown that gaseous inflows are not necessarily common to all interacting systems. Simulations by Mihos & Hernquist (1996), for example, show that galaxy structure plays a role in regulating the gas inflow activity and that the exact nature of an inflow depends on the progenitor bulge-to-disk ratio, the evolutionary phase of the interaction, and the orbital geometry of the encounter. Struck (1997) and Lamb, Hearn, & Gao (1998) have shown that collisions that occur with a more face-on geometry actually produce outwardly expanding gas flows, leaving a central hole in the cool gas distribution of the disk of the target galaxy. Even in the simulations that show inward gas flows, it is not well known how much of this material will remain in the nuclear region, nor is there sufficient resolution or knowledge of the detailed physics of this gas in the existing simulations to know exactly what happens to this gas when it reaches the nucleus. There is also evidence that the spatial distributions of H I and H<sub>2</sub> gas tend to become anti-correlated in interacting systems. As mentioned above, observations have shown that the distribution of molecular gas becomes increasingly concentrated towards the centers of galaxies as an interaction progresses. H I gas, on the other hand, being loosely bound to the galactic disks, tends to get thrown out to large radii (e.g. Hibbard 1995; Wang 1998), leaving depleted levels of atomic gas in the central regions. Therefore it may not be possible to explain the observed increases in H<sub>2</sub> content in the nuclear regions of interacting galaxies as the result of enhanced H I-to-H<sub>2</sub> conversion, because there may not be sufficient quantities of H I near the nuclei to support that process.

All of the preceding results are based on the usual assumption that CO emission serves as a tracer of H<sub>2</sub> and that there is a connection between the velocity-integrated brightness  $I_{\text{CO}}$  of the <sup>12</sup>CO(1–0) line to the column density  $N(\text{H}_2)$  of molecular hydrogen. This includes the assumption that the CO–H<sub>2</sub> connection can be expressed as a constant ratio  $N(\text{H}_2)/I_{\text{CO}}$  in units of molecules  $\text{cm}^{-2}/(\text{K km s}^{-1})$ . The fundamental calibration of this conversion ratio has been done using various observations of Galactic molecular clouds in the solar neighborhood. Recently, however, evidence has been accumulating that the CO–H<sub>2</sub> conversion factor may not be constant with position in a galaxy, nor from galaxy to galaxy.

For example, a radial gradient of more than a factor of 10 has been reported in our Galaxy (Sodroski et al. 1995), and the conversion factor for the central regions of star-

burst galaxies—similar to many of the interacting galaxies in our sample—may differ by as much as two orders of magnitude from that of the dust clouds in the inner disks of quiescent spirals (e.g. Crawford et al. 1985; Stacey et al. 1991; Solomon et al. 1997; Downes & Solomon 1998). These studies suggest that the CO brightness in galaxy disks is largely an excitation effect. We see in general only the skins of the molecular clouds in the emission line of <sup>12</sup>CO(1–0). The observed brightness will therefore depend directly on the excitation temperatures and beam filling factors of the clouds. Furthermore, because  $I_{\text{CO}}/N(\text{H}_2) \propto T/\rho^{1/2}$ , where  $T$  is the gas temperature and  $\rho$  is the density (Dickman, Snell, & Schloerb 1986; Maloney & Black 1988; Elmegreen 1989), an increase in the cloud temperatures will give rise to higher CO luminosities per unit H<sub>2</sub> mass, resulting in overestimates of the H<sub>2</sub> content. Thus the <sup>12</sup>CO(1–0) line will be bright where the ISM is warm, and not necessarily where the H<sub>2</sub> column densities are high.

Observations of nearby quiescent spiral galaxies indicate that the molecular gas in these galaxies is likely to be generally cold and therefore faint in CO emission (Allen et al. 1997; Loinard & Allen 1998). The skins of the molecular clouds may be sufficiently warmed by nearby UV sources to be visible in the <sup>12</sup>CO(1–0) line, but this emission will have a small spatial filling factor, resulting in low observed intensities. In galaxies with higher than normal levels of star formation, like many of the interacting systems in our sample, the intense flux of UV photons from OB stars together with cosmic-rays from supernovae will tend to dissociate the low-density regions of molecular clouds, and the remaining high-density regions will be heated, so that the CO emission lines will emanate from warm, high-density clumps (Allen et al. 1995). Studies of <sup>12</sup>CO/<sup>13</sup>CO and <sup>12</sup>CO(2–1)/<sup>12</sup>CO(1–0) flux ratios in starburst and merging systems do in fact indicate that the CO emission is coming from small, dense, and warm ( $T = 100\text{--}300\text{ K}$ ) clouds (Aalto et al. 1991a,b; Aalto et al. 1995). The observed abundance ratios are significantly higher than those in giant molecular clouds in the Galaxy, and also show radial variations within the galaxies.

Finally, recent studies of the molecular ISM in ultraluminous infrared galaxies have shown that the  $M_{\text{H}_2}/L_{\text{CO}}$  ratio may be 3–5 times lower in the centers of these galaxies than in Galactic molecular clouds (Solomon et al. 1997; Downes & Solomon 1998). Hence the application of the standard CO-to-H<sub>2</sub> conversion factor leads to significant overestimates of the amount of H<sub>2</sub> in these galaxies.

It is possible, therefore, that at least some portion of the effects seen in this study are due to changes in the properties of the molecular gas within the sample galaxies rather than changes in the gas content itself. Instead of the level of star formation activity being driven by molecular gas content, the deduced molecular gas content may be at least partially driven by the level of star formation activity. Portions of the sample of isolated spirals and the subsamples of weakly interacting systems have systematically low levels of current star formation activity. Thus the molecular gas in these galaxies will be cold and the observed level of CO emission low, with potentially large amounts of H<sub>2</sub> remaining unseen. Meanwhile the more strongly interacting systems have overall higher current

star formation rates, which may lead to higher observed levels of CO emission due to increased cloud heating provided by the larger population of young, massive stars.

The increase in observed CO emission in the more active galaxies may be a simple result of having more sites of active star formation within the galaxies, thus increasing the filling factor of warm, CO-emitting regions. At the same time, the large UV and cosmic-ray fluxes provided by massive stars will tend to dissociate the  $H_2$  regions of the clouds, leading to an abnormally high  $I_{CO}/N(H_2)$  ratio and a corresponding overestimate of the mass of  $H_2$  gas. The data in Tables 6 and 8 do in fact show that the average dust temperatures increase with both interaction strength and level of star formation activity. The temperature increase, however, is not very large and the precise connection between observed dust temperatures and molecular gas cloud excitation temperatures is not well known.

The actively star-forming interacting galaxies in the sample studied here appear to have properties that are intermediate between those of the isolated galaxies and the ultraluminous infrared galaxies in other studies. Thus we assume that an intermediate CO-to- $H_2$  conversion factor would be appropriate for these systems. Conversion factors 3 to 5 times lower than the standard have been suggested for the ultraluminous infrared systems, therefore a conversion factor  $\sim 2$  times lower than the standard may be appropriate for the active systems in this study.

A reduction of a factor of 2 in the derived  $H_2$  masses for the galaxies with high SFR's would easily account for the increases in mean  $M_{H_2}/L_B$  and  $M_{H_2}/M_{HI}$  ratios between the low and high SFR subsamples of the interacting systems. Similarly, a factor of 2 reduction in  $M_{H_2}$  for the active interacting class 5 systems would also account for most of the increase in  $M_{H_2}/L_B$  and  $M_{H_2}/M_{HI}$  ratios from class 1 to class 5 systems.

However, changes in the conversion factor of this order cannot account for the whole range of fractional  $H_2$  content seen within the entire isolated and interacting galaxy samples. The  $M_{H_2}/L_B$  and  $M_{H_2}/M_{HI}$  ratios for individual systems cover a range of a factor of 100 in both quantities. Therefore a change in the CO-to- $H_2$  conversion factor on the order of 2 over the range of the samples cannot account for the strong correlation seen between fractional  $H_2$  content and SFR, as measured by  $L_{IR}/L_B$  and  $L_{H\alpha}/L_B$  ratios (see, e.g., Figs. 7 and 9). Therefore even if the apparent increase in the  $H_2$  content of the interacting galaxies—for the sample as a whole relative to the isolated spirals and as a function of SFR and interaction strength—is not real, there still is a correlation between the  $H_2$  content and the current SFR in individual galaxies, for both the isolated and interacting systems.

## 6. SUMMARY

We have analyzed CO (1–0) emission-line observations for a sample of 37 interacting galaxy systems. The parent sample of interacting systems was compiled on the basis of morphological evidence for current involvement in an interaction, without bias towards known optical, infrared, or radio flux levels or indicators of high current SFR's or nuclear activity. The systems in this study were selected from the parent sample in order to span a large range of interaction strengths and star formation properties. If we assume that the CO-to- $H_2$  conversion factor is approxi-

mately constant from galaxy to galaxy within our samples of interacting and isolated galaxies, our results indicate the following.

- 1) There is a good correlation between fractional  $H_2$  content and current SFR's for the overall samples of isolated and interacting galaxies, which indicates that the level of star formation activity is dependent upon the available molecular gas supply in these galaxies.
- 2) Galaxies with high SFR's almost always have moderate to large amounts of  $H_2$  gas and galaxies with low SFR's usually have little to no detectable  $H_2$ . The only exceptions to this are the small number of systems in our “High SFR-Low IR” subsample of interacting systems, which have high current SFR's but little or no detectable far-IR emission or  $H_2$  gas, and a few members of the “Low SFR” subsample which appear to have moderate amounts of  $H_2$ , but very low current SFR's. The apparent lack of  $H_2$  gas in the “High SFR-Low IR” systems may be explained by an anomalous  $H_2/CO$  ratio for the low metallicity ISM in these galaxies. Furthermore, the low metallicity ISM may also be deficient in dust, explaining the lack of thermal far-IR emission from these galaxies. A moderate to large molecular gas supply is therefore a necessary, but not sufficient, condition for spawning significant levels of interaction-induced star formation activity in galaxies.
- 3) A comparison of the relative levels of star formation and  $H_2$  content in the two galaxies within individual interacting pairs shows a correlation between these two properties, but it is weaker than the correlation seen for the overall samples. This indicates that the lack of star formation activity sometimes seen in the individual galaxies of interacting pairs is mainly due to a lack of molecular gas, but also that the specific properties of each interaction event and the galaxies involved must also play a role in governing the level of interaction-induced star formation. This is consistent with some numerical simulations of interacting galaxies that show that interaction-induced gas flows within the galaxies are governed by properties such as bulge-to-disk ratios, collision geometries, and the mass ratios of the galaxies.
- 4) The entire sample of interacting galaxies has a  $L_{IR}/M_{H_2}$  ratio that is a factor of  $\sim 1.3$  higher than that of the isolated spirals, indicating that the rate of high-mass star formation per unit molecular gas—or star formation efficiency—is enhanced in these systems.
- 5) The fractional  $H_2$  content of the whole sample of interacting galaxies, as measured by  $M_{H_2}/L_B$  and  $M_{H_2}/M_{HI}$  ratios, is  $\sim 20$ – $40\%$  higher, on average, than that of the comparison sample of isolated spirals. There is a strong correlation between fractional  $H_2$  content and interaction strength, as determined by degree of morphological disturbance and companion proximity. There is a factor of 2–3 increase in  $M_{H_2}/L_B$  and  $M_{H_2}/M_{HI}$  ratios from the most weakly

interacting to the most strongly interacting systems in our sample. This implies that  $H_2$  is somehow being created in interaction events, and that the process by which this occurs is most pronounced in the most strongly interacting systems. It has been suggested that this is a result of inflows of atomic gas to the central regions of interacting galaxies, and that the large pool of centrally-concentrated dense, cool gas may then be easily converted from atomic to molecular form.

There are indications, however, that the CO-to- $H_2$  conversion factor may not be constant either within individual galaxies or from galaxy to galaxy. Furthermore, the level of observed CO emission itself may be dependent on the level of star formation activity within a galaxy, which will tend to increase the “visibility” of molecular clouds. Reductions in the CO-to- $H_2$  conversion factor that have been suggested for some ultraluminous infrared galaxies would

be more than enough to nullify the average increases in derived  $H_2$  content for the various subsamples of interacting galaxies in this study. They cannot, however, account for the total range of  $H_2$  content seen within the entire samples of isolated and interacting galaxies. Therefore the observed correlation between molecular gas content and current star formation rates must be real.

S.A.L. wishes to thank the Aspen Center for Physics for hospitality during the completion of this work. Portions of this work were carried out at the Jet Propulsion Laboratory, California Institute of Technology, under contract with the National Aeronautics and Space Administration. This research has made use of the NASA/IPAC Extragalactic Database (NED), which is operated by the Jet Propulsion Laboratory, California Institute of Technology, under contract with the National Aeronautics and Space Administration.

## REFERENCES

- Aalto, S., Black, J. H., Booth, R. S., & Johansson, L. E. B. 1991a, *A&A*, 247, 291  
Aalto, S., Black, J. H., Johansson, L. E. B., & Booth, R. S. 1991b, *A&A*, 249, 323  
Aalto, S., Booth, R. S., Black, J. H., & Johansson, L. E. B. 1995, *A&A*, 300, 369  
Allen, R. J., Le Bourlot, J., Lequeux, J., Pineau des Forets, G., & Roueff, E. 1995, *ApJ*, 157, 444  
Allen, R. J., Knapen, J. H., Bohlin, R., & Stecher, T. P. 1997, *ApJ*, 487, 171  
Armus, L., Heckman, T. M., & Miley, G. K. 1990, *ApJ*, 364, 471  
Arnault, P., Casoli, F., Combes, F., & Kunth, D. 1988, *A&A*, 205, 41  
Barnes, J. E., & Hernquist, L. 1992, *ARA&A*, 30, 705  
Barnes, J. E., & Hernquist, L. 1996, *ApJ*, 471, 115  
Biegling, J. H., Blitz, L., Lada, C. J., & Stark, A. A. 1981, *ApJ*, 247, 443  
Bloemen, J. B. G. L., et al. 1986, *A&A*, 154, 25  
Burstein, D., & Heiles, C. 1982, *AJ*, 87, 1165  
Bushouse, H. A. 1986, Ph.D. thesis, University of Illinois  
Bushouse, H. A. 1987, *ApJ*, 320, 49  
Bushouse, H. A., Lamb, S. A., & Werner, M. W. 1988, *ApJ*, 335, 74  
Bushouse, H. A., Telesco, C. M., & Werner, M. W. 1998, *AJ*, 115, 938  
Bushouse, H. A., & Werner, M. W. 1990, *ApJ*, 359, 72  
Casoli, F., Dickey, J., Kazes, I., Boselli, A., Gavazzi, G., & Jore, K. 1996, *A&AS*, 116, 193  
Crawford, M. K., Genzel, R., Townes, C. H., & Watson, D. M. 1985, *ApJ*, 291, 755  
De Vaucouleurs, G., De Vaucouleurs, A., Corwin Jr., H. G., Buta, R. J., Paturel, G., & Fouque, P. 1991, Third Reference Catalogue of Bright Galaxies, Version 3.9 (New York:Springer-Verlag) (RC3)  
Dickman, R. L., Snell, R. L., & Schloerb, F. P. 1986, *ApJ*, 309, 326  
Downes, D., & Solomon, P. M. 1998, *ApJ*, 507, 615  
Elmegreen, B. G. 1989, *ApJ*, 338, 178  
Fullmer, L., & Lonsdale, C. 1989, Cataloged Galaxies and Quasars Observed in the *IRAS* Survey, Version 2 (Pasadena:JPL)  
Gao, Y. 1996, Ph.D. thesis, State Univ. New York, Stony Brook  
Gao, Y., & Solomon, P. M. 1999, *ApJ*, 512, L99  
Garnett, D. R., & Shields, G. A. 1987, *ApJ*, 317, 82  
Gerber, R. A., Lamb, S. A., & Balsara, D. S. 1996, *MNRAS*, 278, 345  
Haynes, M. P., & Giovanelli, R. 1991, *ApJS*, 77, 331  
Hibbard, J. E. 1995, Ph.D. thesis, Columbia University  
Horellou, C., Booth, R. S., & Karlsson, B. 1999, *Ap&SS*, in press  
Huchtmeier, W. K., & Richter, O.-G. 1989, A General Catalog of H I Observations of Galaxies (New York:Springer-Verlag)  
Joseph, R. D., Meikle, W. P. S., Robertson, N. A., & Wright, G. S. 1984, *MNRAS*, 209, 111  
Kaplan, E. L., & Meier, P. 1958, *J. American Stat. Assoc.*, 53, 457  
Kennedy, J. D. P., & Young, J. S. 1989, *ApJ*, 344, 171  
Kennicutt, R. C. 1998, *ARA&A*, 36, 189  
Kleinmann, S. G., & Keel, W. C. 1987, in *Star Formation in Galaxies*, ed. C. J. Lonsdale-Persson, 559 (Washington D.C.:U.S. Govt. Printing Office)  
Lamb, S. A., Gerber, R. A., & Balsara, D. S. 1994, *Ap&SS*, 216, 337  
Lamb, S. A., Hearn, N. C., & Gao, Y. 1998, *ApJ*, 499, L153  
Lo, K. Y., Gao, Y., & Gruendl, R. A. 1997, *ApJ*, 475, L103  
Loinard, L., & Allen, R. J. 1998, *ApJ*, 499, 227  
Madden, S. C., Poglitsch, A., Geis, N., Stacey, G. J., & Townes, C. H. 1997, *ApJ*, 483, 200  
Maloney, P., & Black, J. H. 1988, *ApJ*, 325, 389  
Mihos, J. C., & Hernquist, L. 1996, *ApJ*, 464, 641  
Mihos, J. C., Richstone, D. O., & Bothun, G. D. 1992, *ApJ*, 400, 153  
Mirabel, I. F., & Sanders, D. B. 1989, *ApJ*, 340, L53  
Noguchi, M. 1988, *A&A*, 203, 259  
Noguchi, M. 1991, *MNRAS*, 251, 360  
Olson, K. M., & Kwan, J. 1990, *ApJ*, 361, 426  
Pagel, B. E. J., & Edmunds, M. G. 1981, *ARA&A*, 19, 77  
Richter, O.-G., Sackett, P. D., & Sparke, L. S. 1994, *AJ*, 107, 99  
Sanders, D. B., & Mirabel, I. F. 1985, *ApJ*, 298, L31  
Sanders, D. B., Scoville, N. Z., & Soifer, B. T. 1991, *ApJ*, 370, 158  
Sanders, D. B., Scoville, N. Z., Young, J. S., Soifer, B. T., Schloerb, F. P., Rice, W. L., & Danielson, G. E. 1986, *ApJ*, 305, L45  
Sanders, D. B., Soifer, B. T., Elias, J. H., Madore, B. F., Matthews, K., Neugebauer, G., & Scoville, N. Z. 1988a, *ApJ*, 325, 74  
Sanders, D. B., Soifer, B. T., Elias, J. H., Neugebauer, G., & Matthews, K. 1988b, *ApJ*, 328, L35  
Sanders, D. B., Young, J. S., Scoville, N. Z., Soifer, B. T., & Danielson, G. E. 1987, *ApJ*, 312, L5  
Sargent, A., & Scoville, N. Z. 1991, *ApJ*, 366, L1  
Scoville, N. Z., Sargent, A. I., Sanders, D. B., & Soifer, B. T. 1991, *ApJ*, 366, L5  
Smith, B. J., & Madden, S. C. 1997, *AJ*, 114, 138  
Sodroski, T. J., et al. 1995, *ApJ*, 452, 262  
Sofue, Y., Wakamatsu, K., Taniguchi, Y., & Nakai, N. 1993, *PASJ*, 45, 43  
Soifer, B. T., et al. 1984, *ApJ*, 278, L71  
Solomon, P. M., Downes, D., Radford, S. J. E., & Barrett, J. W. 1997, *ApJ*, 478, 144  
Solomon, P. M., & Sage, L. J. 1988, *ApJ*, 334, 613  
Stacey, G. J., Geis, N., Genzel, R., Lugten, J. B., Poglitsch, A., Sternberg, A., & Townes, C. H. 1991, *ApJ*, 373, 423  
Struck, C. 1997, *ApJS*, 113, 269  
Telesco, C. M., Wolstencroft, R. D., & Done, C. 1988, *ApJ*, 329, 174  
Tinney, C. G., Scoville, N. Z., Sanders, D. B., & Soifer, B. T. 1990, *ApJ*, 362, 473  
Veilleux, S., Kim, D.-C., Sanders, D. B., Mazzarella, J. M., & Soifer, B. T. 1995, *ApJS*, 98, 171  
Vila-Costas, M. B., & Edmunds, M. G. 1992, *MNRAS*, 259, 121  
Wang, W.-H., et al. 1998, *ApJ*, submitted  
Xu, C., & Sulentic, J. W. 1991, *ApJ*, 374, 407  
Young, J. S., Allen, L., Kenney, J. D. P., Lesser, A., & Rownd, B. 1996, *AJ*, 112, 1903  
Young, J. S., Kenney, J. D., Lord, S., & Schloerb, F. P. 1984, *ApJ*, 287, L65  
Young, J. S., & Knezek, 1989, *ApJ*, 347, L55  
Young, J. S., Schloerb, F. P., Kenney, J., & Lord, S. 1986, *ApJ*, 304, 443  
Young, J. S., Xie, S., Kenney, J. D. P., & Rice, W. L. 1989, *ApJS*, 70, 699  
Young, J. S., et al. 1995, *ApJS*, 98, 219  
Zhu, M., Seaquist, E. R., Davoust, E., Frayer, D. T., & Bushouse, H. A. 1999, *AJ*, 118, 145

TABLE 1  
CO DATA FOR INTERACTING SYSTEMS.

Object (1)	Alternate Name (2)	Type (3)	$V_{\text{CO}}$ ( $\text{km s}^{-1}$ ) (4)	$\Delta V_0$ ( $\text{km s}^{-1}$ ) (5)	$\Delta V_{50}$ ( $\text{km s}^{-1}$ ) (6)	$S_{\text{CO}}$ ( $\text{Jy km s}^{-1}$ ) (7)	Ref (8)
Arp 248 a	...	complete	5270	...	...	<42	1
Arp 248 b	...	pair	5120	370	160	67	1
Arp 250 W	...	1 of 2	24200	...	...	<32	1
Arp 256 N	...	complete	8150	160	100	38	1
Arp 256 S	...	pair	8150	330	270	63	1
NGC 1614	Arp 186	merger	4770	390	200	274	1
NGC 4038	...	complete	1540	...	180	1150	2
NGC 4039	...	pair	1570	...	230	920	2
NGC 7592	...	compact	7340	440	300	105	1
UGC 480 W	...	complete	11060	680	330	131	1
UGC 480 E	...	pair	11130	...	...	<32	1
UGC 813	...	complete	5150	$\sim 590$	$\sim 390$	$\sim 68$	1
UGC 816	...	pair	5280	490	270	118	1
UGC 966	NGC 520	merger	2310	...	270	1260	2
UGC 993	...	compact	2880	...	...	<32	1
UGC 1720	IC 214	compact	9080	520	210	88	1
UGC 2320 SW	Arp 190	1 of 2	10390	...	...	<42	1
UGC 2992	...	compact	5030	...	...	<21	1
UGC 3031	NGC 1568a	1 of 2	4690	...	...	<39	1
UGC 3737	...	compact	4440	...	...	<32	1
UGC 4509	NGC 2623	merger	5310	...	170	170	2
UGC 4718 N	NGC 2719	1 of 2	3160	220	...	47	3
UGC 4744 W	NGC 2735	1 of 2	2450	230	...	35	3
UGC 4757	NGC 2744	compact	3440	$\sim 740$	$\sim 290$	$\sim 46$	1
UGC 4881	Arp 55	compact	11950	...	250	200	2
UGC 5617	NGC 3226	complete	1360	...	...	<90	2
UGC 5620	NGC 3227	pair	1110	...	340	450	4
UGC 6224 N	NGC 3561a	complete	8740	450	320	125	1
UGC 6224 S	NGC 3561b	pair	8730	...	...	<49	1
UGC 6471	IC 694	complete	3160	...	250	610	2
UGC 6472	NGC 3690	pair	2930	...	260	290	2
UGC 7776	NGC 4568	complete	2220	260	...	1050	2
UGC 7777	NGC 4567	pair	2280	180	...	500	2
UGC 7938	NGC 4676a	complete	6640	...	390	71	5
UGC 7939	NGC 4676b	pair	6570	...	310	51	5

TABLE 1—*Continued*

Object (1)	Alternate Name (2)	Type (3)	$V_{\text{CO}}$ ( $\text{km s}^{-1}$ ) (4)	$\Delta V_0$ ( $\text{km s}^{-1}$ ) (5)	$\Delta V_{50}$ ( $\text{km s}^{-1}$ ) (6)	$S_{\text{CO}}$ ( $\text{Jy km s}^{-1}$ ) (7)	Ref (8)
UGC 8135	NGC 4922	compact	7060	360	200	74	1
UGC 8335 W	Arp 238 W	complete	9110	...	...	<32	1
UGC 8335 E	Arp 238 E	pair	9310	280	220	~41	1
UGC 8387	IC 883	merger	6960	...	370	220	2
UGC 8528	NGC 5216	complete	2910	...	...	<95	1
UGC 8529	NGC 5218	pair	2940	510	220	350	1
UGC 8641	NGC 5257	complete	6810	530	340	206	1
UGC 8645	NGC 5258	pair	6780	530	390	240	1
UGC 10267	NGC 6090	compact	8870	...	120	200	2
UGC 10923 W	...	complete	7920	220	80	113	1
UGC 10923 E	...	pair	6630	...	...	<32	1
UGC 11175 N	NGC 6621	complete	6170	570	290	170	1
UGC 11175 S	NGC 6622	pair	6230	470	300	103	1
UGC 11284 W	NGC 6670a	complete	8550	570	400	116	1
UGC 11284 E	NGC 6670b	pair	8690	370	230	102	1
UGC 11673 N	...	complete	14270	...	...	<32	1
UGC 11673 S	...	pair	14300	520	370	42	1
UGC 12699	NGC 7714	complete	2860	...	100	130	2
UGC 12700	NGC 7715	pair	2770	...	...	<12	3
UGC 12914	...	complete	4390	690	530	213	1
UGC 12915	...	pair	4490	620	320	502	1

NOTE.—Col. (1) Galaxy name as used in this paper. Col. (2) Alternate name from NGC, Arp, or IC catalogs. Col. (3) Type of system: “complete pair” - CO data for each of two galaxies; “1 of 2” - CO data for one of two galaxies; “compact” - single CO observation of entire system; “merger” - single CO observation of advanced merger. Col. (4) The intensity-weighted mean velocity of the CO line, in units of  $\text{km s}^{-1}$ . Entries for non-detections are the velocity center of the observation. Col. (5) The full width of the CO line, measured at the zero flux level. Col. (6) The full width of the CO line, measured at 50% of the peak line temperature. Col. (7) The CO integrated flux, in units of  $\text{Jy km s}^{-1}$ . Upper limits are  $3\sigma$ . Col. (8) Sources of the CO data: (1) this paper, (2) Young et al. 1995, (3) Sofue et al. 1993, (4) Bieging et al. 1981, (5) Casoli et al. 1996.

TABLE 4  
MEAN AND MEDIAN SAMPLE PROPERTIES.

Quantity	Isolated Galaxies		Interacting Galaxies <sup>a</sup>	
	Mean <sup>b</sup>	Median	Mean <sup>b</sup>	Median
D (Mpc)	23.0±2.3	15.0	85.6±6.9	73.7
$L_B$ ( $10^9 L_\odot$ )	19.5±2.2	12.6	28.9±3.4	23.6
$L_{IR}$ ( $10^9 L_\odot$ )	19.2±4.3	4.1	87.1±14.0	50.7
$M_{HI}$ ( $10^9 M_\odot$ )	3.5±0.5	2.0	7.4±1.0	5.2
$M_{H_2}$ ( $10^9 M_\odot$ )	4.7±0.8	1.8	9.9±1.4	6.4
$\log L_{H\alpha}$ (ergs/s)	41.12±0.06	40.95	41.57±0.10	41.18
$\log S_{60}/S_{100}$	-0.37±0.02	-0.36	-0.30±0.02	-0.29
$T_{dust}$ (K)	33.6±0.4	33.4	35.7±0.7	35.5
$L_{IR}/L_B$	0.74±0.09	0.46	2.30±0.42	1.00
$L_{H\alpha}/L_B$	0.0022±0.0002	0.0018	0.0033±0.0004	0.0023
$L_{IR}/M_{H_2}$ ( $L_\odot/M_\odot$ )	4.8±0.5	3.4	6.8±1.1	4.1
$L_{H\alpha}/M_{H_2}$ ( $L_\odot/M_\odot$ )	0.016±0.002	0.011	0.016±0.002	0.012
$M_{HI}/L_B$ ( $M_\odot/L_\odot$ )	0.24±0.03	0.15	0.29±0.04	0.22
$M_{H_2}/L_B$ ( $M_\odot/L_\odot$ )	0.20±0.02	0.15	0.36±0.05	0.23
$M_{H_2}/M_{HI}$	1.98±0.35	1.01	1.85±0.26	1.45

<sup>a</sup>Quantities involving *IRAS* measurements are global values for each interacting system. All others use values for individual galaxies, when available.

<sup>b</sup>Mean values have been computed using the Kaplan-Meier estimator of a randomly censored distribution, which properly accounts for non-detections. The quoted errors are the  $1\sigma$  uncertainty in the mean.

TABLE 5  
INTERACTING GALAXY SUBSAMPLE MEMBERS.

High SFR-High IR	High SFR-Low IR	Low SFR
NGC 1614	UGC 993	Arp 250 W
UGC 4509	UGC 2992	UGC 480 W
UGC 4881	UGC 3737	UGC 480 E
UGC 6471/2	UGC 4757	UGC 2320 SW
UGC 8335		UGC 3031
UGC 8387		UGC 11673 N
UGC 11284		UGC 11673 S

TABLE 6  
MEAN PROPERTIES OF INTERACTING SUBSAMPLES SELECTED BY SFR.

Quantity <sup>a</sup>	Low SFR	High SFR, Low IR	High SFR, High IR
Number of systems	5	4	7
$L_B$ ( $10^9 L_\odot$ )	$48.0 \pm 21.6$	$5.9 \pm 1.9$	$40.7 \pm 10.8$
$L_{\text{IR}}$ ( $10^9 L_\odot$ )	$39.0 \pm 15.7$	$< 3.9 \pm 1.6$	$232.8 \pm 18.1$
$M_{\text{HI}}$ ( $10^9 M_\odot$ )	$6.6 \pm 2.9$	$3.8 \pm 0.7$	$9.7 \pm 4.5$
$M_{\text{H}_2}$ ( $10^9 M_\odot$ )	$< 16.8 \pm 5.3$	$< 0.9 \pm 0.2$	$22.2 \pm 7.1$
$\log L_{\text{H}\alpha}$ (ergs/s)	$40.83 \pm 0.30$	$40.88 \pm 0.12$	$41.82 \pm 0.13$
$\log S_{60}/S_{100}$	$-0.51 \pm 0.06$	$-0.26 \pm 0.07$	$-0.15 \pm 0.04$
$T_{\text{dust}}$ (K)	$29.9 \pm 1.4$	$36.4 \pm 2.3$	$40.2 \pm 1.4$
$L_{\text{IR}}/L_B$	$0.61 \pm 0.20$	$< 0.59 \pm 0.15$	$6.90 \pm 0.90$
$L_{\text{H}\alpha}/L_B$	$0.0002 \pm 0.0001$	$0.0043 \pm 0.0016$	$0.0044 \pm 0.0012$
$L_{\text{IR}}/M_{\text{H}_2}$ ( $L_\odot/M_\odot$ )	$> 2.0 \pm 0.5$	$> 3.8 \pm 1.5$	$16.1 \pm 4.6$
$L_{\text{H}\alpha}/M_{\text{H}_2}$ ( $L_\odot/M_\odot$ )	$> 0.001 \pm 0.001$	$> 0.021 \pm 0.006$	$0.012 \pm 0.005$
$M_{\text{HI}}/L_B$ ( $M_\odot/L_\odot$ )	$0.18 \pm 0.08$	$0.56 \pm 0.20$	$0.32 \pm 0.16$
$M_{\text{H}_2}/L_B$ ( $M_\odot/L_\odot$ )	$< 0.43 \pm 0.10$	$< 0.20 \pm 0.06$	$0.67 \pm 0.20$
$M_{\text{H}_2}/M_{\text{HI}}$	$< 1.70 \pm 0.91$	$< 0.29 \pm 0.04$	$3.44 \pm 0.80$

<sup>a</sup>Quantities involving IRAS measurements are global values for each interacting system. All others use values for individual galaxies, when available.

TABLE 7  
INTERACTION STRENGTH CLASSIFICATIONS.

Class 1	Class 2	Class 3	Class 4	Class 5
UGC 5617/20	Arp 248	Arp 256	NGC 4038/9	NGC 1614
UGC 7776/7	Arp 250	UGC 813/6	NGC 7592	UGC 966
	UGC 480	UGC 993	UGC 1720	UGC 4509
	UGC 2320	UGC 2992	UGC 3737	UGC 8387
	UGC 3031	UGC 6224	UGC 4757	
	UGC 8528/9	UGC 7938/9	UGC 4881	
	UGC 11673	UGC 8135	UGC 6471/2	
	UGC 12914/5	UGC 8335	UGC 10267	
		UGC 8641/5	UGC 12699/700	
		UGC 10923		
		UGC 11175		
		UGC 11284		

TABLE 8  
MEAN PROPERTIES OF INTERACTION CLASS SUBSAMPLES.

Quantity <sup>a</sup>	Class 1	Class 2	Class 3	Class 4	Class 5
Number of systems	2	8	12	9	4
$L_B$ ( $10^9 L_\odot$ )	33.3±21.6	56.0±21.1	51.6±14.0	38.5±9.7	22.9±1.5
$L_{\text{IR}}$ ( $10^9 L_\odot$ )	19.1±22.0	35.5±9.6	101.8±24.3	113.9±39.1	161.9±44.5
$M_{\text{HI}}$ ( $10^9 M_\odot$ )	4.2±3.6	6.3±1.4	11.4±2.8	9.1±2.3	4.5±1.2
$M_{\text{H}_2}$ ( $10^9 M_\odot$ )	7.9±9.5	17.8±6.6	17.6±3.7	20.1±7.5	14.0±3.0
$\log L_{\text{H}\alpha}$ (ergs/s)	41.37±0.63	41.37±0.37	41.75±0.16	41.83±0.20	41.48±0.30
$\log S_{60}/S_{100}$	−0.44±0.16	−0.46±0.05	−0.25±0.03	−0.23±0.04	−0.17±0.06
$T_{\text{dust}}$ (K)	31.4±3.3	31.0±1.1	36.7±0.9	37.3±1.3	39.5±2.1
$L_{\text{IR}}/L_B$	0.45±0.37	0.69±0.12	2.3±0.7	2.5±0.7	7.0±1.8
$L_{\text{H}\alpha}/L_B$	0.0016±0.0011	0.0010±0.0006	0.0040±0.0008	0.0042±0.0007	0.0032±0.0018
$L_{\text{IR}}/M_{\text{H}_2}$ ( $L_\odot/M_\odot$ )	2.7±0.4	3.4±0.9	9.3±3.5	8.6±1.9	12.5±3.9
$L_{\text{H}\alpha}/M_{\text{H}_2}$ ( $L_\odot/M_\odot$ )	0.010±0.003	0.008±0.007	0.012±0.003	0.021±0.007	0.006±0.004
$M_{\text{HI}}/L_B$ ( $M_\odot/L_\odot$ )	0.12±0.04	0.18±0.04	0.28±0.10	0.35±0.09	0.20±0.06
$M_{\text{H}_2}/L_B$ ( $M_\odot/L_\odot$ )	0.18±0.17	0.27±0.08	0.37±0.11	0.44±0.17	0.61±0.13
$M_{\text{H}_2}/M_{\text{HI}}$	1.44±1.04	2.38±1.56	1.93±0.44	2.41±0.92	3.39±0.51

<sup>a</sup>All quantities have been computed using global values for each interacting system.

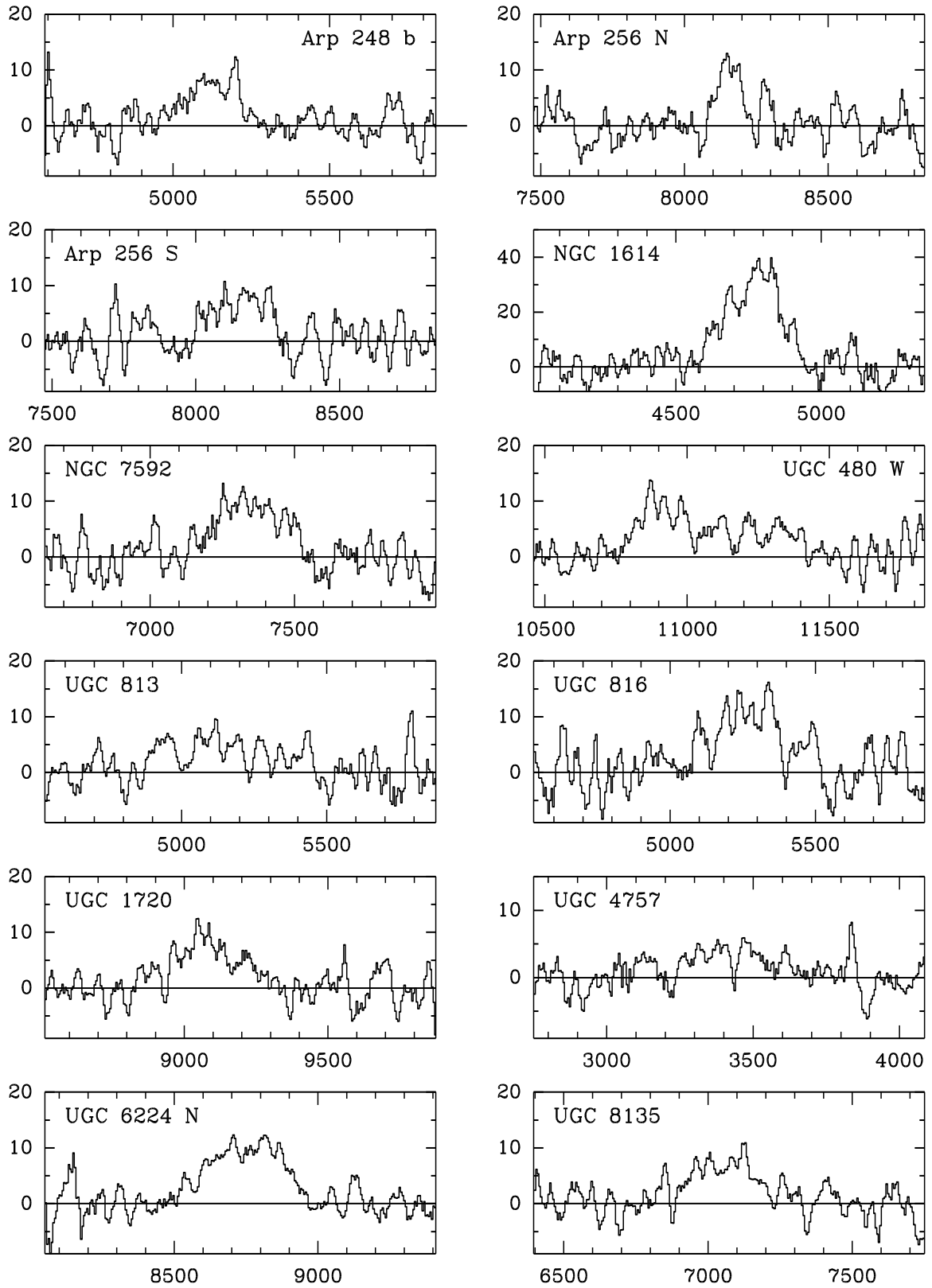


FIG. 1.— CO spectra of the interacting galaxies. The intensity scale is in units of  $T_R^*$  (mK). The  $x$ -axis is redshift expressed in units of  $\text{km s}^{-1}(cz)$ .

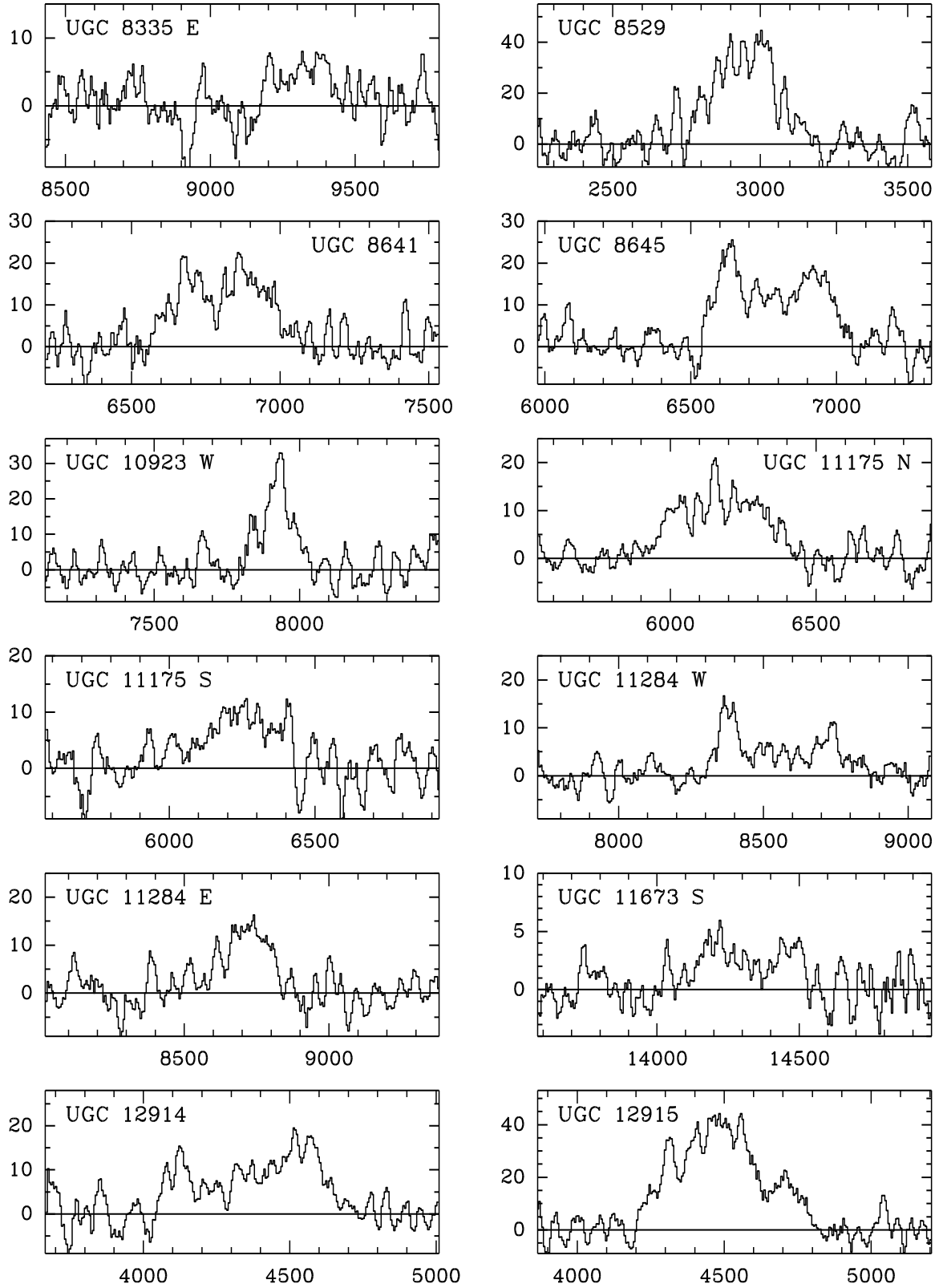


FIG. 1.— (continued)

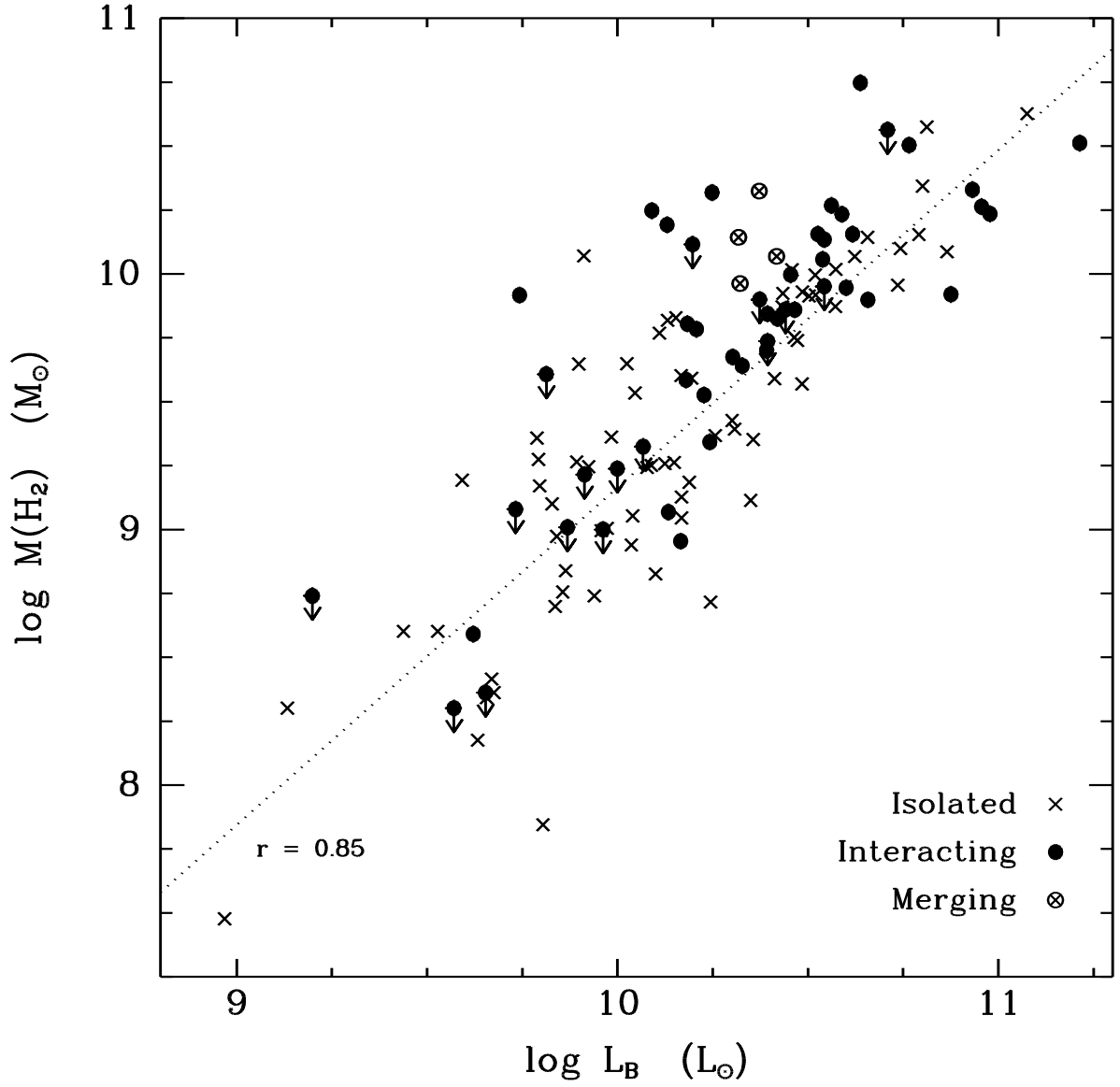


FIG. 2.—  $\text{H}_2$  gas content as a function of optical blue luminosity for the isolated and interacting galaxies. The dotted line is a linear fit to the isolated galaxy data only and  $r$  is the correlation coefficient. Values for the interacting systems are for individual galaxies, when available, otherwise they are totals for a system.

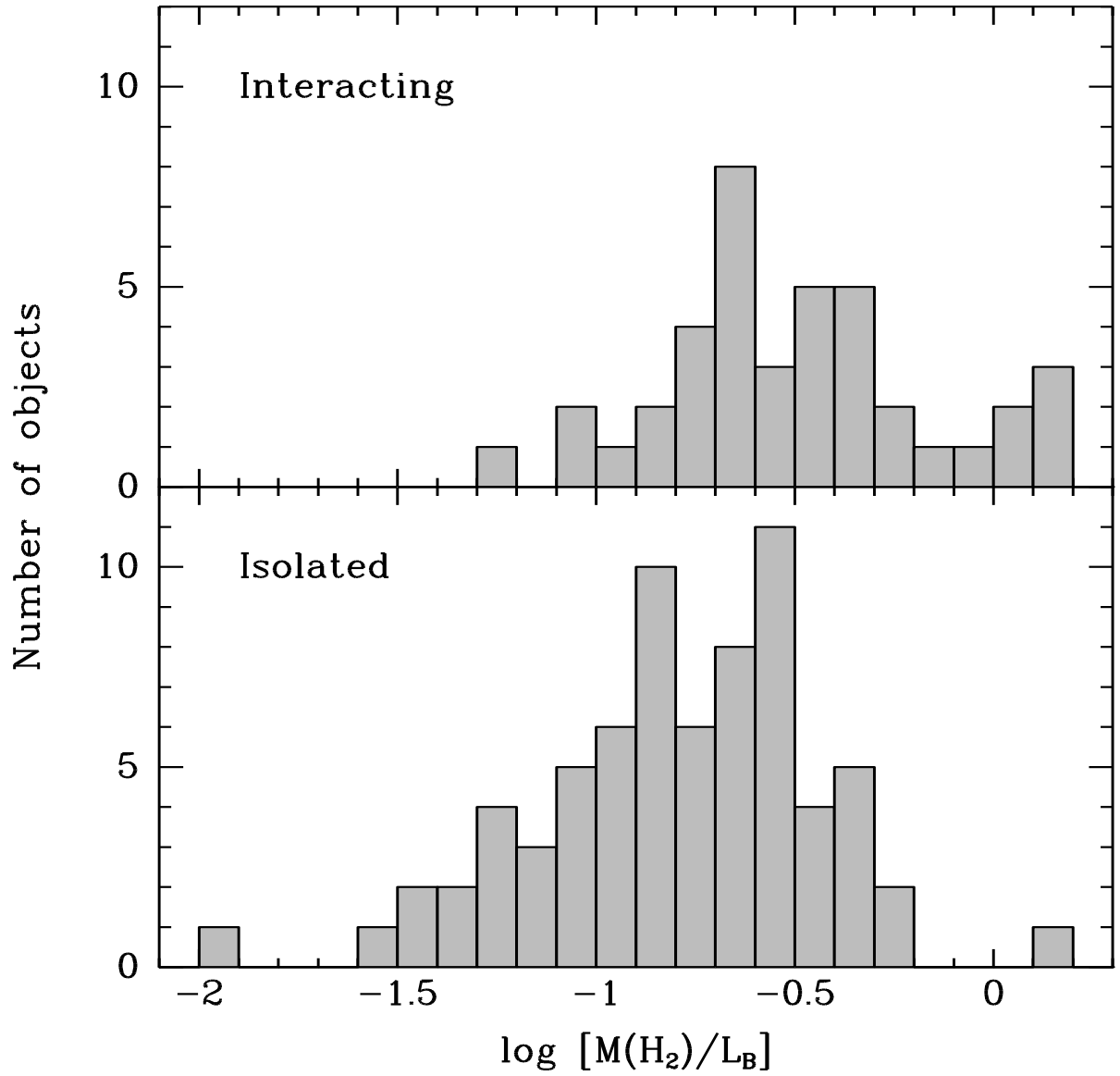


FIG. 3.— Distributions of  $\text{H}_2$  mass to blue luminosity ratios for the isolated and interacting galaxies. Values for the interacting systems are for individual galaxies, when available, otherwise they are averages for a system.

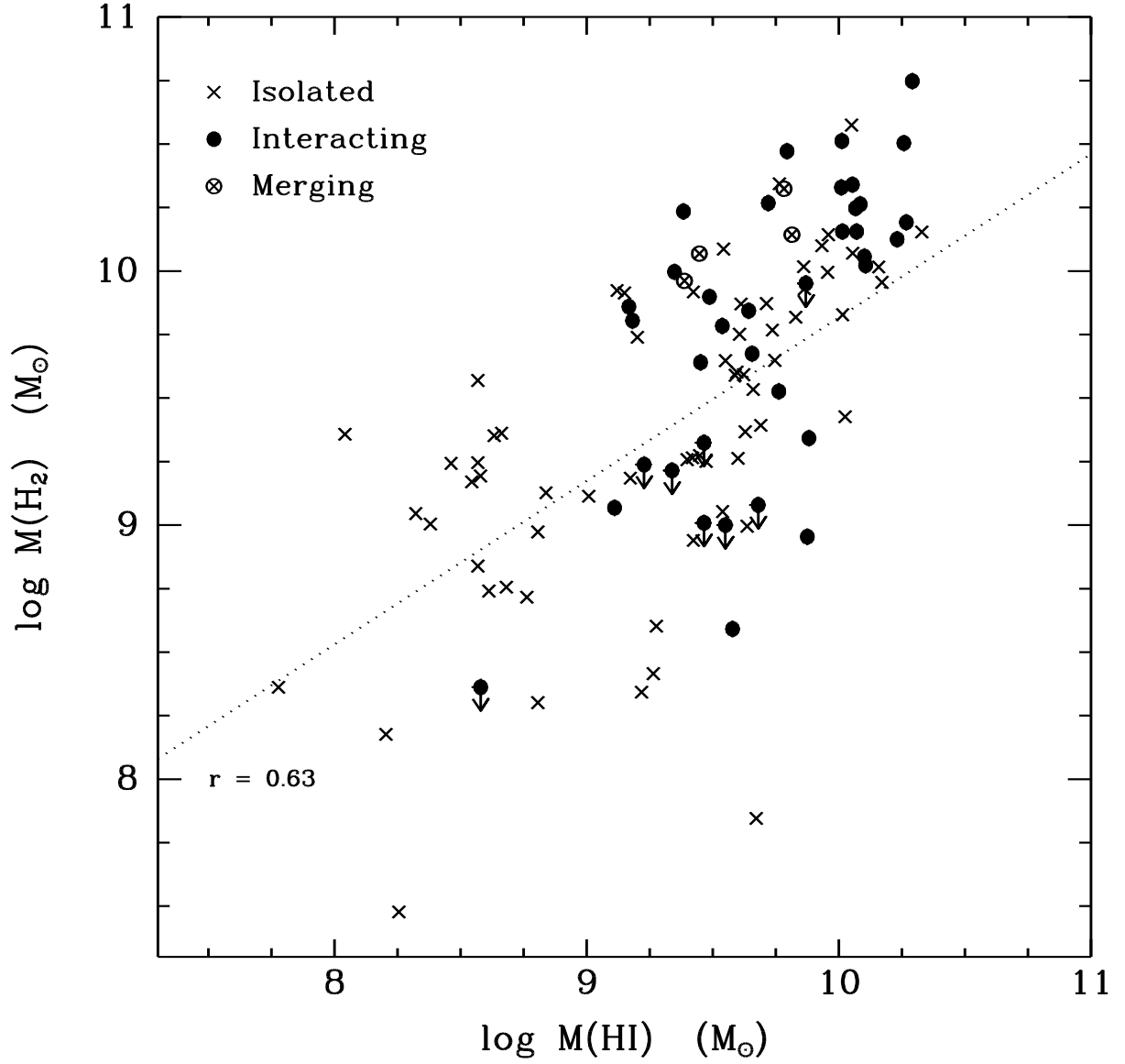


FIG. 4.—  $\text{H}_2$  gas content as a function of  $\text{H I}$  gas content for the isolated and interacting galaxies. The dotted line is a linear fit to the isolated galaxy data only and  $r$  is the correlation coefficient. Values for the interacting systems are for individual galaxies, when available, otherwise they are totals for a system.

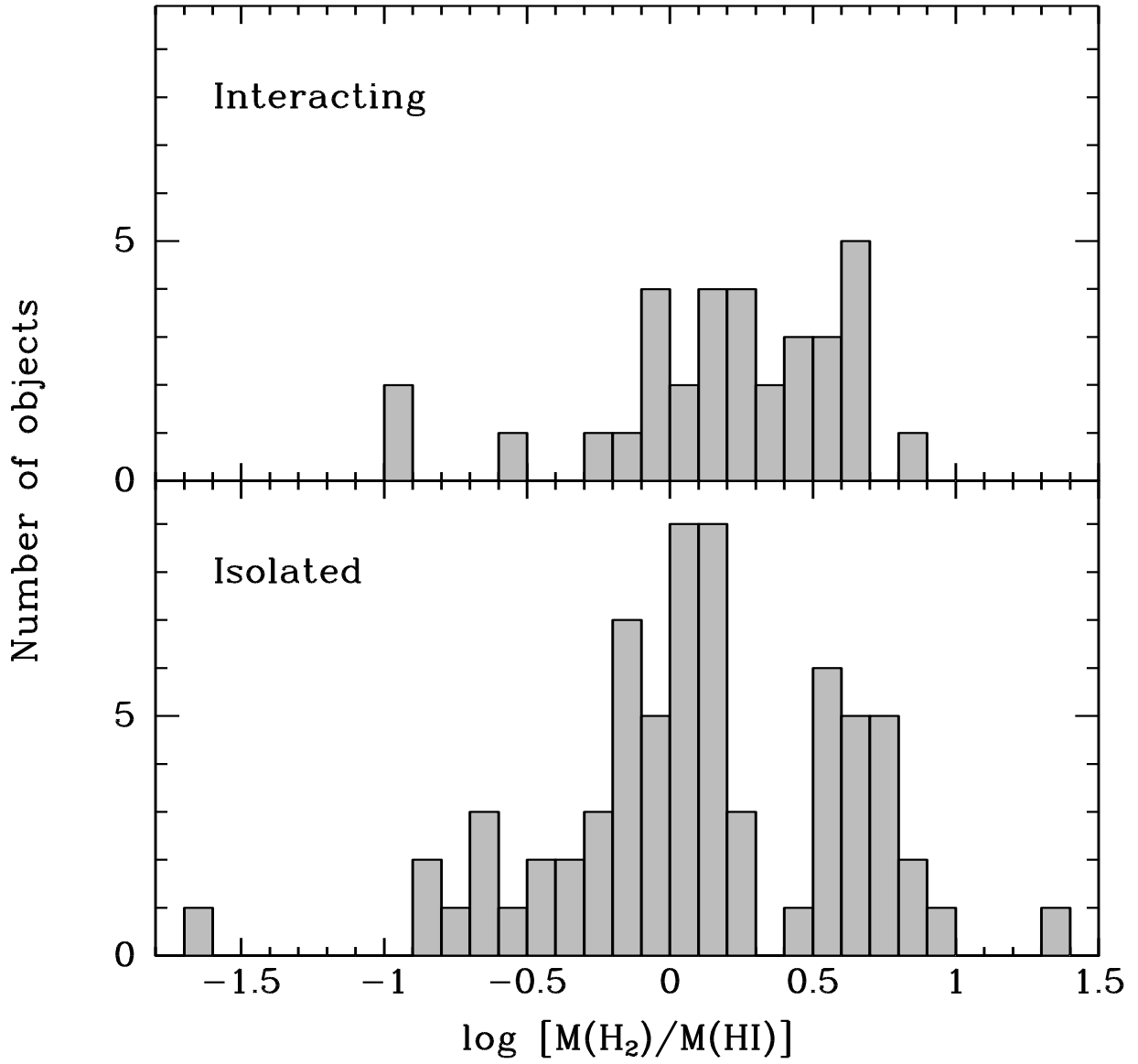


FIG. 5.— Distributions of  $\text{H}_2$  to  $\text{H I}$  mass ratios for the isolated and interacting galaxies. Values for the interacting systems are for individual galaxies, when available, otherwise they are averages for a system.

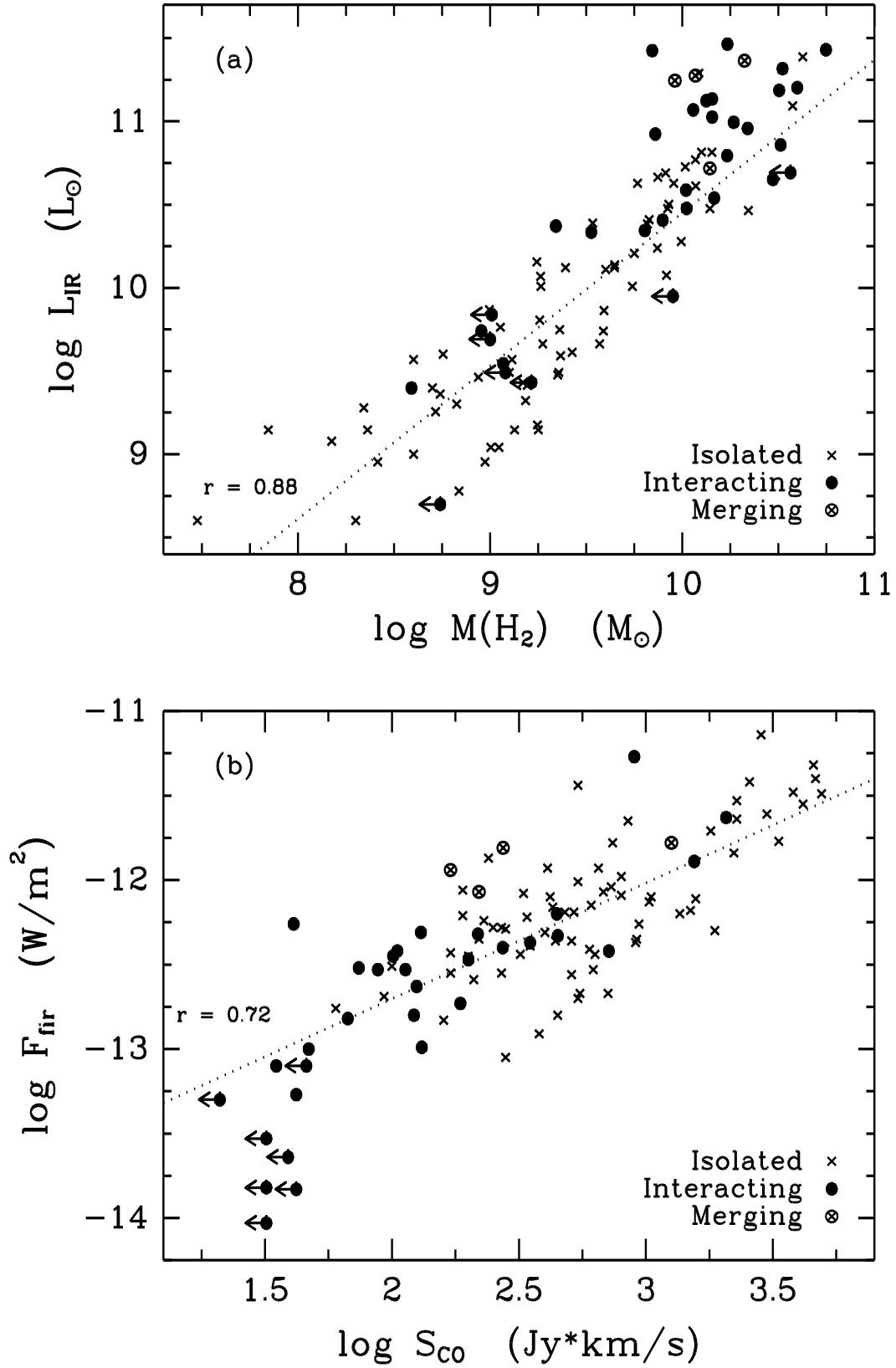


FIG. 6.— (a) Far-infrared luminosity versus H<sub>2</sub> content and (b) far-infrared versus CO flux for the isolated and interacting galaxies. The dotted lines are linear fits to the isolated galaxy data only and  $r$  is the correlation coefficient. All values for the interacting galaxies are totals for a system.

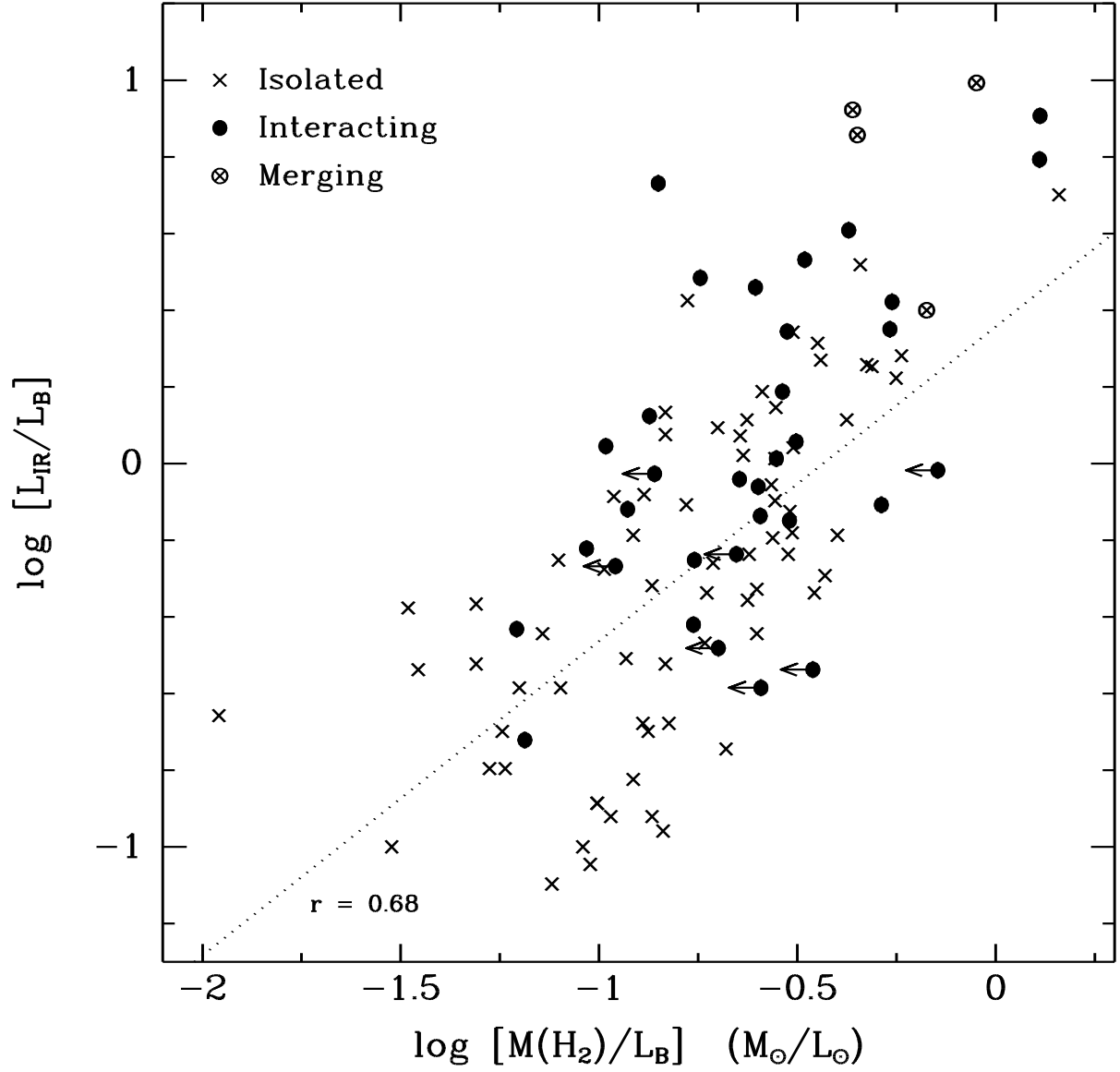


FIG. 7.— Far-infrared to blue luminosity ratio versus the molecular gas to blue luminosity ratio for the isolated and interacting galaxies. The dotted line is a linear fit to the isolated galaxy data only and  $r$  is the correlation coefficient. All values for the interacting galaxies are averages for a system.

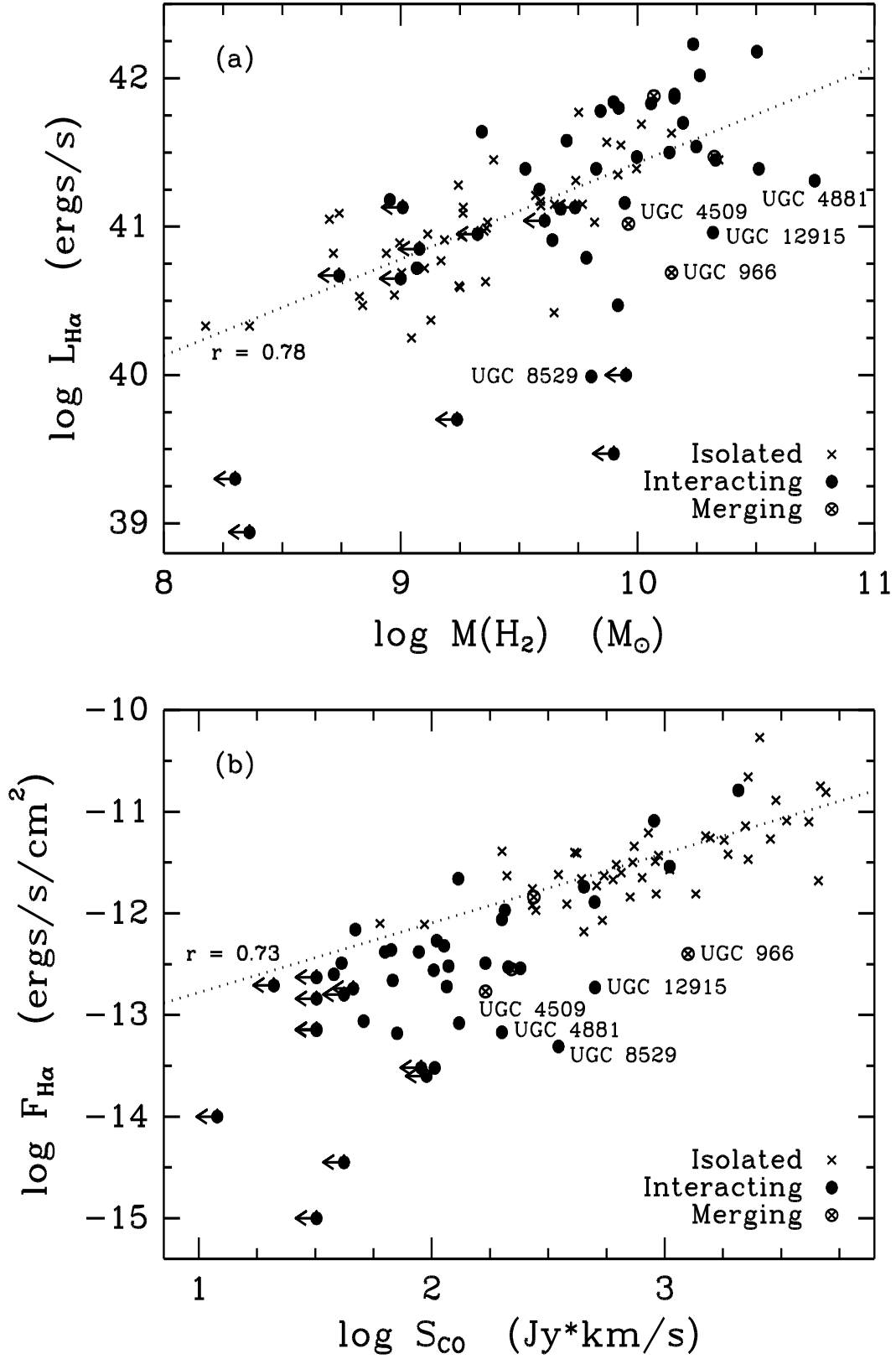


FIG. 8.— (a) H $\alpha$  luminosity versus H $_2$  content and (b) H $\alpha$  versus CO emission fluxes for the isolated and interacting galaxies. The dotted lines are linear fits to the isolated galaxy data only and  $r$  is the correlation coefficient. Values for the interacting systems are for individual galaxies, when available, otherwise they are totals for a system.

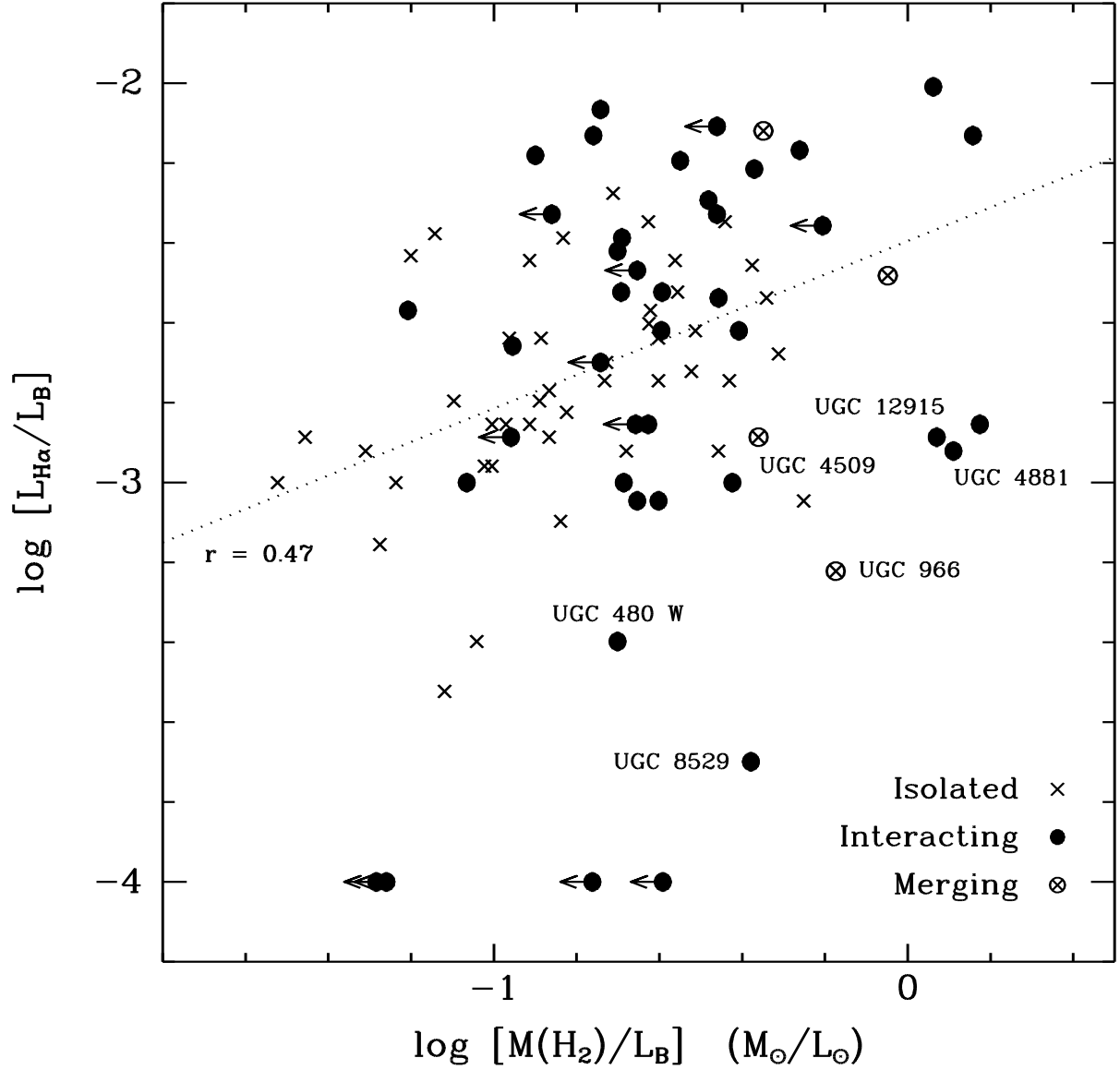


FIG. 9.— H $\alpha$  to blue luminosity ratio versus H $_2$  gas mass to blue luminosity ratio for the isolated and interacting galaxies. The dotted line is a linear fit to the isolated galaxy data only and  $r$  is the correlation coefficient. Values for the interacting systems are for individual galaxies, when available, otherwise they are the global average for a system.

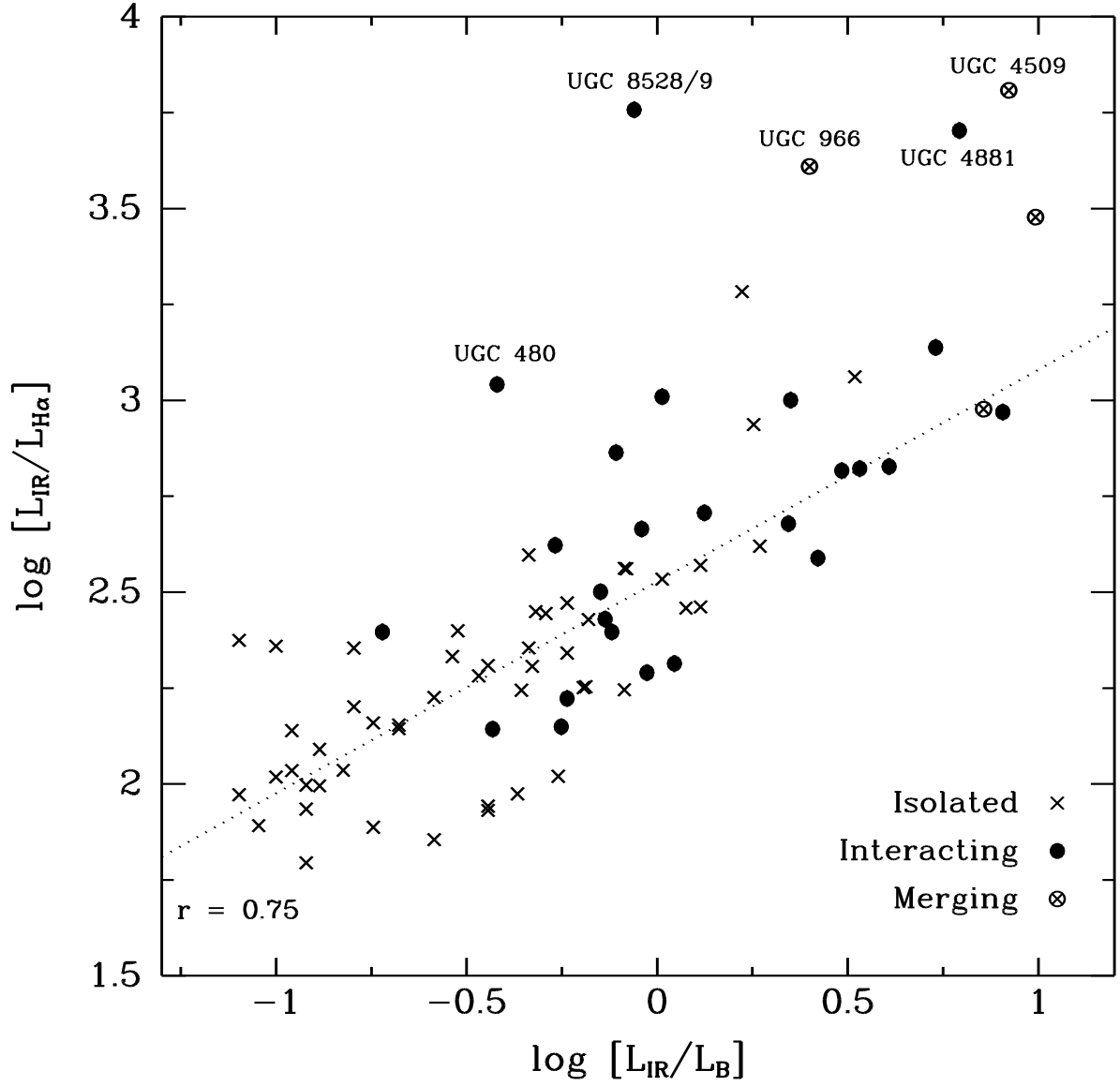


FIG. 10.— Far-infrared to H $\alpha$  luminosity ratio versus far-infrared to blue luminosity ratio for the isolated and interacting galaxies. The dotted line is a linear fit to the isolated galaxy data only and  $r$  is the correlation coefficient. All values for the interacting systems are global averages for each system.

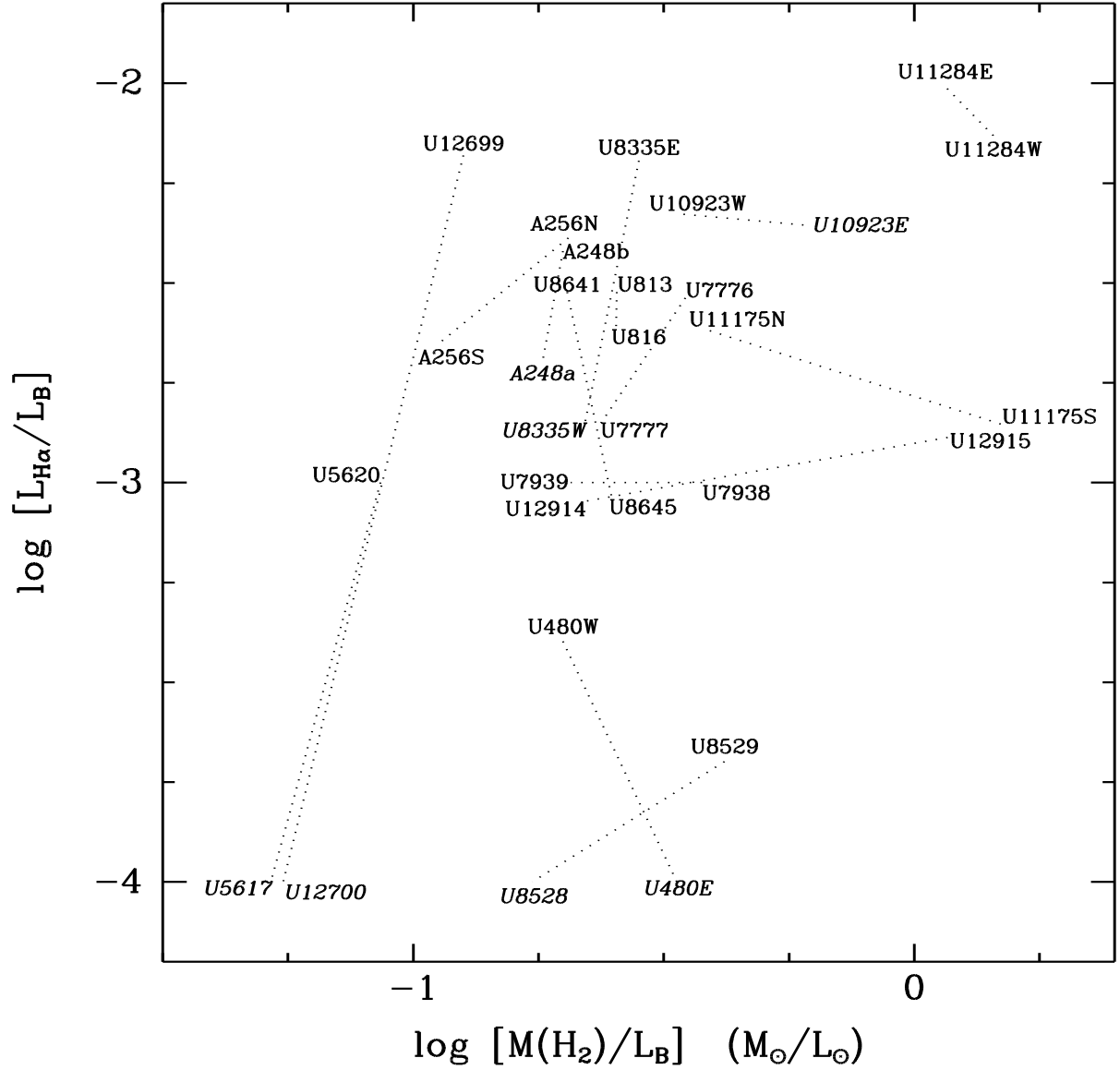


FIG. 11.— H $\alpha$  to blue luminosity ratio versus H $_2$  gas mass to blue luminosity ratio for individual interacting pairs. All values are derived from measurements of the individual galaxies. Object names in italic font indicate CO non-detections and therefore the  $M_{H_2}/L_B$  data point represents an upper-limit.

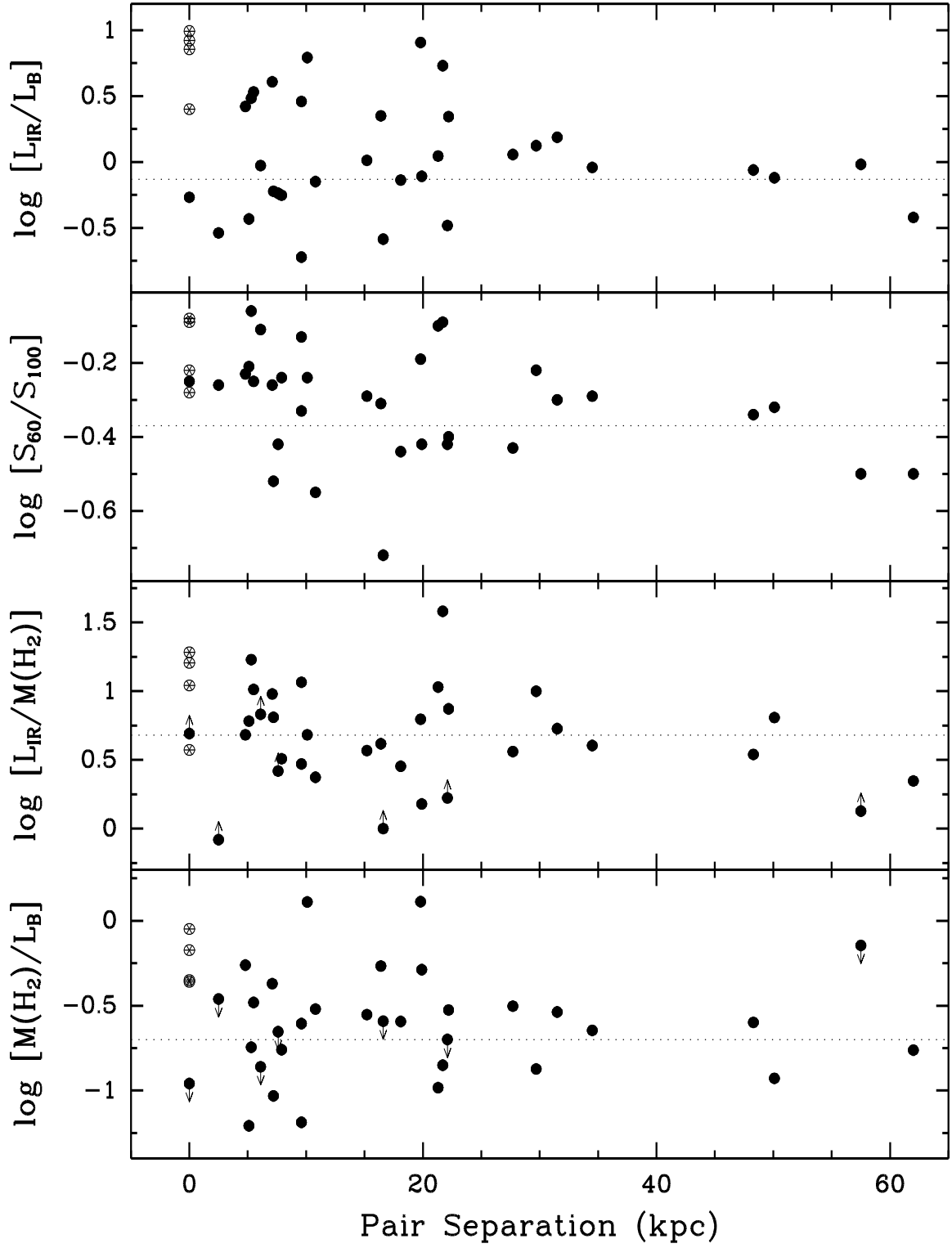


FIG. 12.— Interacting galaxy characteristics as a function of projected pair separation. All values are global averages for each system. The dotted line in each panel shows the mean value for the sample of isolated galaxies.

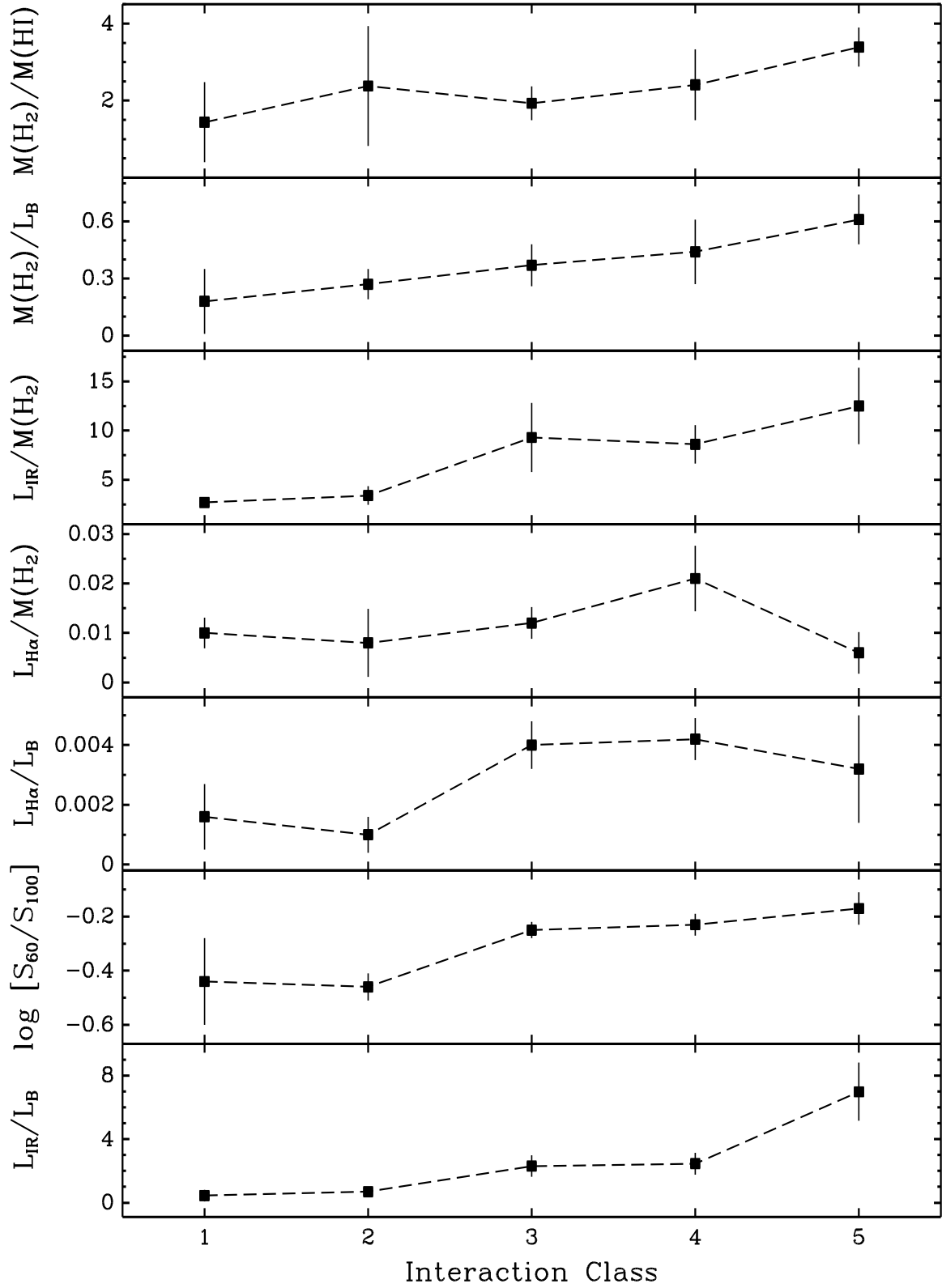


FIG. 13.— Mean characteristics as a function of interaction class. Error bars are the  $1\sigma$  uncertainty in the mean.

TABLE 2  
OBSERVED DATA FOR INTERACTING SYSTEMS.

Object (1)	$V_0$ (km/s) (2)	$B_T$ (mag) (3)	$A_B$ (mag) (4)	$S_{CO}$ (Jy km/s) (5)	$S_{60}$ (Jy) (6)	$S_{100}$ (Jy) (7)	$\log F_{IR}$ (W/m <sup>2</sup> ) (8)	$S_{HI}$ (Jy km/s) (9)	H I Ref (10)	$\log F_{H\alpha}$ (erg/cm <sup>2</sup> /s) (11)	H $\alpha$ Ref (12)
Arp 248a	5139	14.50	0.04	<42	2.59	5.41	-12.82	2.71	1	-12.80	1b
Arp 248b	4993	14.10	0.04	67				5.37	1	-12.36	1b
Arp 250 W	24181	16.42	0.17	<32	0.21	0.67	-13.82	...	...	...	...
Arp 256 N	8219	14.81	0.11	38	6.70	11.1	-12.45	6.01	1	-12.60	1a
Arp 256 S	8215	13.60	0.11	63						-12.38	1a
NGC 1614	4676	13.63	0.22	274	32.4	39.0	-11.81	3.05	1	-11.84	2
NGC 4038	1382	10.91	0.05	1150	43.5	75.0	-11.63	37.42	2	-10.79	2
NGC 4039	1414	11.08	0.05	920							
NGC 7592	7452	14.22	0.10	105	6.92	12.2	-12.42	5.42	1	-12.27	1a
UGC 480 W	11228	13.50	0.17	131	1.40	4.4	-12.99	<1.93	1	-13.08	1a
UGC 480 E	11302	15.60	0.17	<32						-15.00	1a
UGC 813	5316	14.80	0.49	68	2.76	7.58	-12.73	10.50	1	-12.66	1a
UGC 816	5449	14.20	0.49	118						-12.52	1a
UGC 966	2376	12.24	0.05	1260	31.1	51.7	-11.78	27.53	2	-12.40	2
UGC 993	2958	15.60	0.14	<32	0.17	<0.31	<-14.03	...	...	-12.63	1b
UGC 1720	9120	14.70	0.11	88	5.26	9.59	-12.53	2.96	1	-12.38	1a
UGC 2320 SW	10432	15.20	0.36	<42	0.15	<0.78	<-13.83	1.62	1	-14.45	1a
UGC 2992	4983	15.40	0.48	<21	1.03	1.33	-13.30	2.80	1	-12.71	1b
UGC 3031	4632	14.90	0.25	<39	0.35	0.93	-13.64	2.42	1	...	...

TABLE 2—*Continued*

Object (1)	$V_0$ (km/s) (2)	$B_T$ (mag) (3)	$A_B$ (mag) (4)	$S_{CO}$ (Jy km/s) (5)	$S_{60}$ (Jy) (6)	$S_{100}$ (Jy) (7)	$\log F_{IR}$ (W/m <sup>2</sup> ) (8)	$S_{HI}$ (Jy km/s) (9)	H I Ref (10)	$\log F_{H\alpha}$ (erg/cm <sup>2</sup> /s) (11)	H $\alpha$ Ref (12)
UGC 3737	4379	15.30	0.32	<32	0.45	1.18	−13.53	5.95	1	−12.84	1b
UGC 4509	5248	13.99	0.09	170	24.0	29.2	−11.94	2.11	1	−12.77	3
UGC 4718 N	3133	13.25	0.08	47	1.88	3.03	−13.00	18.22	2	−12.16	1b
UGC 4744 W	2385	14.04	0.10	35	1.06	3.52	−13.10	15.90	1	...	...
UGC 4757	3342	13.90	0.08	<46	1.45	2.59	−13.10	7.58	1	−12.74	1b
UGC 4881	11959	14.90	0.00	200	6.18	10.8	−12.47	3.26	1	−13.17	4
UGC 5617	1278	12.30	0.02	<90	7.84	16.9	−12.33	6.79	3	−13.52	1b
UGC 5620	1028	11.10	0.02	450				23.14	2	−11.74	1b
UGC 6224 N	8710	14.40	0.00	125	4.06	8.17	−12.63	1.65	1	...	...
UGC 6224 S	8699	14.70	0.00	<49						...	...
UGC 6471	3237	11.80	0.00	610	114.	129.	−11.27	5.90	1	−11.09	2
UGC 6472	3011	11.98	0.00	290							
UGC 7776	2168	11.68	0.00	1050	16.7	59.3	−11.89	10.98	2	−11.54	2
UGC 7777	2230	12.06	0.00	500				22.32	2	−11.89	2
UGC 7938	6652	14.70	0.01	71	2.76	5.41	−12.80	1.88	1	−13.18	1b
UGC 7939	6582	14.40	0.01	51				1.54	1	−13.06	1b
UGC 8135	7074	14.20	0.01	74	6.17	8.23	−12.52	0.70	3	...	...
UGC 8335 W	9233	15.00	0.03	<32	11.4	14.1	−12.26	1.20	3	−13.14	1b
UGC 8335 E	9433	15.00	0.03	41						−12.49	1b
UGC 8387	7000	14.40	0.00	220	15.2	28.8	−12.07	2.95	4	−12.55	5
UGC 8528	3039	13.56	0.03	<95	7.02	15.5	−12.37	4.31	5	−13.60	1b
UGC 8529	3067	13.10	0.03	350				3.88	5	−13.31	1b

TABLE 2—*Continued*

Object (1)	$V_0$ (km/s) (2)	$B_T$ (mag) (3)	$A_B$ (mag) (4)	$S_{\text{CO}}$ (Jy km/s) (5)	$S_{60}$ (Jy) (6)	$S_{100}$ (Jy) (7)	$\log F_{\text{IR}}$ (W/m <sup>2</sup> ) (8)	$S_{\text{HI}}$ (Jy km/s) (9)	H I Ref (10)	$\log F_{\text{H}\alpha}$ (erg/cm <sup>2</sup> /s) (11)	H $\alpha$ Ref (12)
UGC 8641	6761	12.87	0.01	206	11.0	21.5	−12.20	6.37	1	−11.97	1a
UGC 8645	6727	12.93	0.01	240				5.36	1	−12.54	1a
UGC 10267	9032	13.97	0.00	200	6.27	10.6	−12.47	5.29	1	−12.06	1b
UGC 10923 W	8098	14.30	0.21	113	4.65	11.7	−12.53	4.33	1	−12.32	1a
UGC 10923 E	7993	16.31	0.21	<32						−13.15	1a
UGC 11175 N	6369	14.00	0.22	170	6.78	13.8	−12.40	6.58	1	−12.49	1a
UGC 11175 S	6436	16.00	0.22	103						−13.52	1a
UGC 11284 W	8757	15.80	0.19	116	9.20	14.3	−12.32	3.56	1	−12.72	1a
UGC 11284 E	8904	15.70	0.19	102				5.66	1	−12.56	1a
UGC 11673 N	14428	16.66	0.25	<32	0.80	2.15	−13.27	...	...	...	...
UGC 11673 S	14450	15.68	0.25	42				...	...	...	...
UGC 12699	2983	13.00	0.16	130	10.0	12.7	−12.31	21.00	1	−11.66	1b
UGC 12700	2895	14.68	0.16	<12						−14.00	1b
UGC 12914	4555	13.07	0.15	213	5.77	15.0	−12.42	7.00	1	−12.53	1a
UGC 12915	4653	13.95	0.15	502						−12.73	1a

NOTE.— Col. (1) Galaxy name. Col. (2) Galactocentric velocity, assuming  $V_0 = V_\odot + 9\cos(l)\cos(b) + 232\sin(l)\cos(b) + 7\sin(b)$  (De Vaucouleurs et al. 1991: RC3). Col. (3) Total blue magnitude from the RC3 or UGC catalogs. Col. (4) Galactic extinction from Burstein & Heiles 1982. Col. (5) CO flux from Tables 1 and 2. Cols. (6)–(7) *IRAS* flux densities at 60 and 100  $\mu\text{m}$ . All measurements are totals for each system and are listed only for the first object in a pair. Col. (8) Far-infrared flux computed according to  $F_{\text{IR}} = 1.26(2.58 \times 10^{-14} S_{60} + 1 \times 10^{-14} S_{100})$ , using the 60 and 100  $\mu\text{m}$  fluxes from columns 6 and 7. Col. (9) H I flux. Measurements that are totals for a system are listed only for the first object in a pair. Col. (10) Sources of the H I data: (1) Bushouse 1987, (2) RC3, (3) Huchtmeier & Richter 1989, (4) Richter, Sackett, & Sparke 1994, (5) Haynes & Giovanelli 1991. Col. (11) H $\alpha$  flux. Measurements that are totals for a system are listed only for the first object in a pair. Col. (12) Sources of the H $\alpha$  data: (1a) Bushouse 1987—narrow-band imaging, (1b) Bushouse 1987—22'' aperture spectrophotometry, (2) Young et al. 1996—narrow-band imaging, (3) Armus, Heckman, & Miley 1990—narrow-band imaging, (4) Veilleux et al. 1995—long-slit spectrophotometry, (5) Kennicutt 1998—narrow-band imaging.

TABLE 3  
DERIVED DATA FOR INTERACTING SYSTEMS.

Object	$D$ (Mpc)	$L_B$ ( $10^9 L_\odot$ )	$L_{\text{IR}}$ ( $10^9 L_\odot$ )	$M_{\text{H}_2}$ ( $10^9 M_\odot$ )	$M_{\text{HI}}$ ( $10^9 M_\odot$ )	$\frac{L_{\text{IR}}}{L_B}$	$\frac{L_{\text{IR}}}{M_{\text{H}_2}}$ ( $\frac{L_\odot}{M_\odot}$ )	$\frac{M_{\text{H}_2}}{L_B}$ ( $\frac{M_\odot}{L_\odot}$ )	$\frac{M_{\text{H}_2}}{M_{\text{HI}}}$	log $L_{\text{H}\alpha}$ (ergs/s)	$\frac{L_{\text{H}\alpha}}{L_B}$	$\frac{L_{\text{H}\alpha}}{M_{\text{H}_2}}$ ( $\frac{L_\odot}{M_\odot}$ )
(1)	(2)	(3)	(4)	(5)	(6)	(7)	(8)	(9)	(10)	(11)	(12)	(13)
Arp 248a	68	11.7	21.6	<2.1	2.9	0.8	6.4	<0.18	<0.72	40.95	0.0020	>0.011
Arp 248b		16.9		3.4	5.8			0.20	0.58	41.39	0.0038	0.019
Arp 250 W	322	51.2	49.2	<36.6	...	1.0	>1.3	<0.72	...	...	...	...
Arp 256 N	110	24.6	133.1	5.0	17.0	1.3	10.0	0.20	0.78	41.58	0.0041	0.020
Arp 256 S		75.0		8.3				0.11		41.80	0.0022	0.020
NGC 1614	62	26.2	188.2	11.7	2.8	7.2	16.1	0.45	4.19	41.88	0.0076	0.017
NGC 4038	19	24.5	25.5	4.4	3.1	0.6	3.2	0.18	2.58	41.84	0.0074	0.041
NGC 4039		20.9		3.5				0.17				
NGC 7592	99	34.6	117.3	11.4	12.6	3.4	10.3	0.33	0.90	41.83	0.0051	0.015
UGC 480 W	150	163.4	72.2	32.5	<10.3	0.4	2.2	0.20	>3.16	41.39	0.0004	0.002
UGC 480 E		23.6		<7.9				<0.34		39.47	<0.0001	>0.001
UGC 813	72	15.1	30.0	3.9	12.8	0.7	2.8	0.26	0.83	41.25	0.0030	0.012
UGC 816		26.3		6.7				0.25		41.39	0.0024	0.010
UGC 966	32	20.8	52.1	13.9	6.5	2.5	3.7	0.67	2.13	40.69	0.0006	0.001
UGC 993	39	1.6	<0.5	<0.6	...	<0.3	~0.8	<0.35	...	40.67	0.0078	>0.023
UGC 1720	122	33.6	136.4	14.3	10.3	4.1	9.5	0.43	1.39	41.89	0.0061	0.014
UGC 2320 SW	139	34.9	<8.9	<8.9	7.4	<0.3	~1.0	<0.26	<1.21	40.00	0.0001	>0.001
UGC 2992	66	7.4	6.9	<1.0	2.9	0.9	>6.8	<0.14	<0.35	41.13	0.0047	>0.034
UGC 3031	62	8.2	2.7	<1.6	2.2	0.3	>1.7	<0.20	<0.75	...	...	...

TABLE 3—*Continued*

Object	$D$ (Mpc)	$L_B$ ( $10^9 L_\odot$ )	$L_{\text{IR}}$ ( $10^9 L_\odot$ )	$M_{\text{H}_2}$ ( $10^9 M_\odot$ )	$M_{\text{HI}}$ ( $10^9 M_\odot$ )	$\frac{L_{\text{IR}}}{L_B}$	$\frac{L_{\text{IR}}}{M_{\text{H}_2}}$ ( $\frac{L_\odot}{M_\odot}$ )	$\frac{M_{\text{H}_2}}{L_B}$ ( $\frac{M_\odot}{L_\odot}$ )	$\frac{M_{\text{H}_2}}{M_{\text{HI}}}$	$\log L_{\text{H}\alpha}$ (ergs/s)	$\frac{L_{\text{H}\alpha}}{L_B}$	$\frac{L_{\text{H}\alpha}}{M_{\text{H}_2}}$ ( $\frac{L_\odot}{M_\odot}$ )
(1)	(2)	(3)	(4)	(5)	(6)	(7)	(8)	(9)	(10)	(11)	(12)	(13)
UGC 3737	58	5.4	3.1	<1.2	4.8	0.6	>2.6	<0.22	<0.25	40.85	0.0034	>0.015
UGC 4509	70	21.0	175.7	9.2	2.4	8.4	19.2	0.44	3.75	41.02	0.0013	0.003
UGC 4718 N	42	14.7	5.5	0.9	7.5	0.4	6.1	0.06	0.12	41.18	0.0027	0.044
UGC 4744 W	32	4.2	2.5	0.4	3.8	0.6	6.5	0.09	0.10	...	...	...
UGC 4757	45	9.2	4.9	<1.0	3.6	0.5	>4.9	<0.11	<0.28	40.65	0.0013	>0.012
UGC 4881	160	43.4	269.3	55.9	19.6	6.2	4.8	1.29	2.86	41.31	0.0012	0.001
UGC 5617	15	4.5	3.5	<0.2	0.4	0.2	3.0	<0.05	<0.61	38.94	0.0001	>0.001
UGC 5620		13.6		1.2	1.3			0.09	0.91	40.72	0.0010	0.012
UGC 6224 N	116	36.4	98.7	18.5	5.3	1.5	5.3	0.51	3.53	...	...	...
UGC 6224 S		27.6		<7.3				<0.26		...	...	...
UGC 6471	42	51.4	291.2	11.6	2.4	3.1	17.0	0.23	7.10	42.23	0.0086	0.038
UGC 6472		43.6		5.5				0.13				
UGC 7776	29	28.5	34.6	9.9	2.2	0.7	2.4	0.35	4.45	41.47	0.0029	0.008
UGC 7777		20.1		4.7	4.5			0.24	1.04	41.12	0.0014	0.006
UGC 7938	88	16.1	38.6	6.1	3.5	1.0	3.7	0.38	1.76	40.79	0.0010	0.003
UGC 7939		21.2		4.4	2.8			0.21	1.54	40.91	0.0010	0.005
UGC 8135	94	29.2	84.0	7.2	1.5	2.9	11.6	0.25	4.93	...	...	...
UGC 8335 W	124	24.8	266.0	<5.5	4.4	5.4	38.1	<0.22	1.59	41.13	0.0014	>0.007
UGC 8335 E		24.8		7.0				0.28		41.78	0.0064	0.023
UGC 8387	93	23.6	231.7	21.1	6.1	9.8	11.0	0.90	3.48	41.47	0.0033	0.004
UGC 8528	41	10.0	22.1	<1.7	1.7	0.9	3.5	<0.17	<1.02	39.70	0.0001	>0.001
UGC 8529		15.3		6.4	1.5			0.42	4.20	39.99	0.0002	<0.001

TABLE 3—*Continued*

Object	$D$ (Mpc)	$L_B$ ( $10^9 L_\odot$ )	$L_{\text{IR}}$ ( $10^9 L_\odot$ )	$M_{\text{H}_2}$ ( $10^9 M_\odot$ )	$M_{\text{HI}}$ ( $10^9 M_\odot$ )	$\frac{L_{\text{IR}}}{L_B}$	$\frac{L_{\text{IR}}}{M_{\text{H}_2}}$ ( $\frac{L_\odot}{M_\odot}$ )	$\frac{M_{\text{H}_2}}{L_B}$ ( $\frac{M_\odot}{L_\odot}$ )	$\frac{M_{\text{H}_2}}{M_{\text{HI}}}$	log $L_{\text{H}\alpha}$ (ergs/s)	$\frac{L_{\text{H}\alpha}}{L_B}$	$\frac{L_{\text{H}\alpha}}{M_{\text{H}_2}}$ ( $\frac{L_\odot}{M_\odot}$ )
(1)	(2)	(3)	(4)	(5)	(6)	(7)	(8)	(9)	(10)	(11)	(12)	(13)
UGC 8641	90	90.3	159.4	18.3	12.2	0.9	4.0	0.20	1.51	42.02	0.0030	0.015
UGC 8645		85.5		21.4	10.2			0.25	2.09	41.45	0.0009	0.003
UGC 10267	120	58.3	153.6	31.9	18.1	2.6	4.8	0.55	1.76	42.18	0.0068	0.012
UGC 10923 W	107	41.4	106.2	14.3	11.8	2.2	7.4	0.35	1.22	41.87	0.0047	0.014
UGC 10923 E		6.5		<4.1				<0.62		41.04	0.0044	>0.007
UGC 11175 N	85	34.9	90.7	13.6	11.3	2.2	4.1	0.39	1.93	41.50	0.0024	0.006
UGC 11175 S		5.5		8.3				1.49		40.47	0.0014	0.001
UGC 11284 W	118	12.3	207.4	17.7	11.7	8.1	6.2	1.44	1.52	41.54	0.0074	0.005
UGC 11284 E		13.5		15.6	18.5			1.15	0.84	41.70	0.0098	0.009
UGC 11673 N	193	15.7	62.2	<13.1	...	1.1	3.6	<0.83	...	...	...	...
UGC 11673 S		38.8		17.1	...			0.44		...	...	...
UGC 12699	39	17.5	23.5	2.2	7.6	1.1	10.7	0.13	0.29	41.64	0.0066	0.052
UGC 12700		3.7		<0.2				<0.06		39.30	0.0001	>0.003
UGC 12914	61	39.8	44.8	8.8	6.2	0.8	1.5	0.22	4.76	41.16	0.0009	0.004
UGC 12915		17.7		20.8				1.18		40.96	0.0013	0.001

NOTE.— Col. (1) Galaxy name. Col. (2) Distance in Mpc, computed using the mean  $V_0$  of each system from Table 2, and assuming  $H_0 = 75 \text{ km s}^{-1} \text{ Mpc}^{-1}$ . Col. (3) Blue luminosity, computed from values of  $B_T$  in Table 2, corrected for Galactic extinction, and assuming  $M_{B_\odot} = +5.48$ . Col. (4) Far-infrared luminosity, computed from values of  $F_{\text{IR}}$  in Table 2. Measurements are totals for each system and are listed only for the first object in a pair. This applies to all quantities involving *IRAS* far-infrared measurements. Col. (5)  $\text{H}_2$  mass, computed using  $M_{\text{H}_2} = 1.1 \times 10^4 D^2 S_{\text{CO}}$ . Col. (6)  $\text{H I}$  mass, computed using  $M_{\text{HI}} = 2.36 \times 10^5 D^2 S_{\text{HI}}$ . Measurements that are totals for a system are listed only for the first object in a pair. Col. (7) Far-infrared to blue luminosity ratio. Col. (8) Far-infrared luminosity to  $\text{H}_2$  mass ratio. Col. (9)  $\text{H}_2$  mass to blue luminosity ratio. Col. (10)  $\text{H}_2$  to  $\text{H I}$  mass ratio. Measurements that are averages for a system are listed only for the first object in a pair. Col. (11) Logarithm of the  $\text{H}\alpha$  luminosity. Measurements that are totals for a system are listed only for the first object in a pair. Col. (12)  $\text{H}\alpha$  to blue luminosity ratio. Col. (13)  $\text{H}\alpha$  luminosity to  $\text{H}_2$  mass ratio.